





THE COHERENCE OF THE OCEANIC HEAT TRANSPORT THROUGH THE NORDIC SEAS: OCEANIC HEAT BUDGET AND INTERANNUAL VARIABILITY

Anna V. Vesman^{*,1,2} , Igor L. Bashmachnikov^{1,3} , Pavel A. Golubkin³ , and Roshin P. Raj⁴ 

¹Saint-Petersburg State University, Department of Oceanography, Saint-Petersburg, Russian Federation

²Arctic and Antarctic research institute, Atmosphere-sea ice-ocean interaction department, Saint-Petersburg, Russian Federation

³Nansen International Environmental and Remote Sensing Centre, Saint-Petersburg, Russian Federation

⁴Nansen Environmental and Remote Sensing Centre, Bjerknes Center for climate Research, Bergen, Norway

* Correspondence to: Anna V. Vesman, anna.vesman@gmail.com

Abstract: The Atlantic Water is the main source of heat and salt in the Arctic. Properties of the Atlantic Water inflow regionally affect sea ice extent and deep water formation rate. The Atlantic Water heat transported into the Nordic Seas has a significant impact on the local climate and is investigated here along with its inter-annual variability. We use the ARMOR3D dataset, which is a collection of 3D monthly temperature, salinity and geostrophic velocities fields, derived from in situ and satellite data on a regular grid available since 1993. We compare the heat transport across seven zonal transects in the eastern part of the Nordic seas, from the Svinøy section (65°N) to the Fram Strait (78.8°N). The correlations of the interannual variations of the advective heat fluxes rapidly drop from Svinøy to Jan Mayen sections and between Bear Island and Sørkapp sections. This is a result of different tendencies in its interannual evolution over the latest decades in the southern and the northern parts of the study region, as well as of a differential damping of the observed periodicities along the Atlantic Water path on its way north (the amplitude of 5–6 year oscillations drops significantly faster than that of 2–3 year oscillations). A certain link between the heat fluxes and the North Atlantic Oscillation (NAO), Arctic Oscillation (AO) and East Atlantic (EA) indices is observed only at the southern sections. On the other hand, the heat fluxes at all sections show a consistent increase during the dominance of western weather type W and a decrease – of meridional weather type C. The link is explained by the variations of the wind fields, favorable for the sea-level build-up (Ekman pumping) east of the branching of the Norwegian Current for type W and an opposite tendency for type C.

Keywords: the Nordic Seas, the Atlantic Water, heat flux, correlation loss, long-term variability.

Citation: Vesman, A. V., I. L. Bashmachnikov, P. A. Golubkin, and R. P. Raj (2023), The Coherence of the Oceanic Heat Transport Through the Nordic Seas: Oceanic Heat Budget and Interannual Variability, *Russ. J. Earth. Sci.*, 23, ES3006, <https://doi.org/10.2205/2023es000848>

RESEARCH ARTICLE

Received: 13 December 2022

Accepted: 24 April 2023

Published: 18 August 2023



Copyright: © 2023. The Authors. This article is an open access article distributed under the terms and conditions of the Creative Commons Attribution (CC BY) license (<https://creativecommons.org/licenses/by/4.0/>).

1. Introduction

The Arctic region is undergoing significant changes in 20–21 centuries. Among other factors, interannual variations of temperature, sea ice extent and etc. in the Arctic region are linked to variability in the poleward transport of heat by the ocean and the atmosphere, often coupled [Bashmachnikov et al., 2018; Buckley and Marshall, 2016; Jungclaus and Koenigk, 2009; Schlichtholz, 2011]. A significant amount of the northward directed oceanic heat is released in the Nordic Seas and in the Whaler's Bay north of Spitsbergen [Bosse et al., 2018; Moore et al., 2012; Piechura and Walczowski, 2009; Smedsrud et al., 2013]. Previously, the subsurface Atlantic water (AW) was believed not to affect the Arctic climate after submerging and entering the Arctic [Lenn et al., 2009; Rudels et al., 2013; Sirevaag and Fer, 2012]. However, recent studies show that the AW can reach the upper mixed layer in the

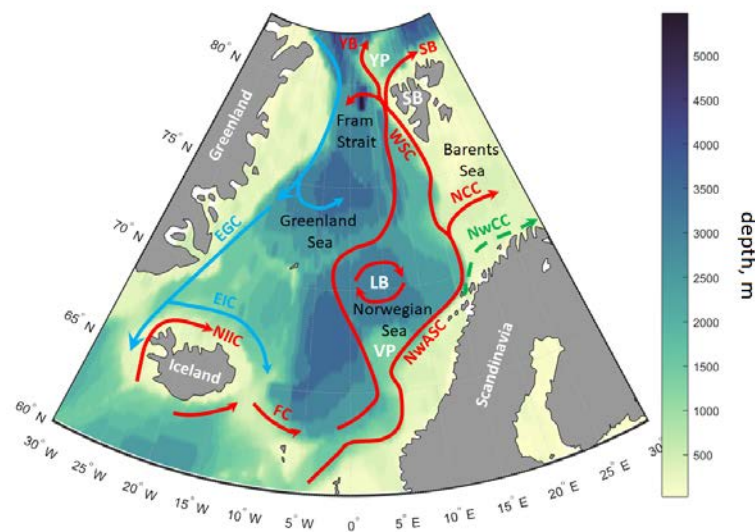


Figure 1. Schematic map of oceanic circulation in the study region, NwASC – Norwegian Atlantic Slope Current (NwASC), NwAFC – Norwegian Atlantic Front Current, NwCC – Norwegian Coastal Current, NCC – North Cape Current, WSC – West Spitsbergen Current, SB – Svalbard branch, YB – Yermak branch, EGC – East Greenland Current, EIC – East Icelandic Current, NIIC – North Icelandic Irminger Current, SIC – South Icelandic Current, FC – Faroe Current; VP – Vøring plateau, LB – Lofoten basin, Sb – Spitsbergen, YP – Yermak plateau.

Atlantic sector of the Arctic (which is a result of the recent AW warming), thus becoming an important factor for the Arctic climate change [Carmack *et al.*, 2015; Polyakov *et al.*, 2017; Schlichtholz, 2013; Tverberg *et al.*, 2014].

The warm and saline AW is transported north across the Nordic Seas (Figure 1) by the Norwegian Atlantic Slope Current (NwASC) along the continental margin of Norway and by the Norwegian Atlantic Front Current (NwAFC) along the Jan Mayen Fracture zone and Mohn–Knipovich ridges [Orvik and Niiler, 2002; Poulain *et al.*, 1996; Skagseth *et al.*, 2004]. There is practically no AW transport from the Barents Sea to the Arctic Ocean [Makhotin and Ivanov, 2016; Smedsrud *et al.*, 2013], most of the oceanic heat enters the Arctic Ocean through the Fram Strait [Beszczynska-Möller *et al.*, 2015; Rudels, 1987, 2015; Schauer *et al.*, 2004]. The West Spitsbergen Current (WSC), a continuation of the NwASC, has a complex structure near the Fram Strait, where it is split into several branches and recirculations [Aagaard *et al.*, 1987; Gascard *et al.*, 1995; von Appen *et al.*, 2015]. Two main branches enter the Arctic, the Svalbard branch along the Spitsbergen slope (limited by the 400 m isobath) and the Yermak branch along the western flank of the Yermak Plateau, while several recirculation branches turns southwestwards into the Greenland Sea [Cokelet *et al.*, 2008; Saloranta and Haugan, 2004; von Appen *et al.*, 2015].

When entering the Nordic Seas, the Faroe, East Icelandic and West Icelandic currents merge together (Figure 1) to carry a total of about 8–9 Sv into the Norwegian Current, including both, the NwAFC and the NwASC [Dickson *et al.*, 2008; Rossby *et al.*, 2018]. The associated heat flux is estimated of a total of 260–300 TW (reference $T = 0^\circ\text{C}$) of heat advected with the AW into the eastern Norwegian Sea [Hansen *et al.*, 2008; Rossby *et al.*, 2018]. Further on, on its way through the Nordic Seas to the Arctic Basin, the AW undergoes a dispersion in several recirculations and density transformations through its heat loss to the atmosphere and mixing with the surrounding waters [Bosse *et al.*, 2018; Chafik *et al.*, 2016; Muilwijk *et al.*, 2018; Polyakov *et al.*, 2017]. Across the Svinøy section located several degrees further north in the Norwegian Sea, the Norwegian Current carries an average of 4–6 Sv [Mork and Skagseth, 2010] and around 150 TW of heat (the estimates vary from 100 to 200 TW, [Bacon *et al.*, 2015; Skagseth *et al.*, 2008]). Therefore, approximately half of the

incoming AW heat is released to the atmosphere or heats the Arctic waters coming from the Greenland Sea, even before it reaches the Lofoten Basin known as a region with an exceptionally large winter heat loss [Segtman *et al.*, 2011].

The AW further enters the Barents Sea along the northern shelf of Scandinavia as the North Cape and the Norwegian Coastal (Murmansk) currents with a total average transport of 2 Sv (from 1 to 3 Sv [Smedsrud *et al.*, 2013]); the average annual oceanic heat flux into the Barents Sea (reference $T = 0^{\circ}\text{C}$) is around 50 TW (ranging from 30 to 70 TW, [Bashmachnikov *et al.*, 2018; Skagseth *et al.*, 2008, 2011; Smedsrud *et al.*, 2010]. Since 1998, a monotonous increase of around 1.5 TW per year is observed. This is associated with an increase in the volume transport, rather than a growth of the AW temperature [Kalavichchi and Bashmachnikov, 2019; Schauer *et al.*, 2008]. The volume and heat fluxes are re-distributed between the Barents Sea and the Fram Strait, governed by the regional wind patterns forming the sea-level anomalies via convergences/divergences of Ekman fluxes [Lien *et al.*, 2013].

The WSC transport increased during recent decades from 3 to 8 Sv (in the southern Fram Strait) and is 6–11 Sv in the northern Fram Strait, with a characteristic inter-annual variability of about 5 Sv [Beszczynska-Möller *et al.*, 2015; Fahrbach, 2006; Rudels *et al.*, 2013; Schauer *et al.*, 2004, 2008]. Some differences in the estimates may be due to a complex flow structure and difficulty in evaluating an effect of strong local recirculations. Considering a relatively stable AW transport of about 2 Sv [Beszczynska-Möller *et al.*, 2015], the intensification of the WSC is thought to be fed by an entrainment of the Greenland Sea Water [Walczowski, 2014]. The total northwards heat flux through the Fram Strait is around 30 TW [Walczowski, 2014], i.e., only 10% of the total heat entering the Norwegian Sea reaches the Fram Strait. About the same amount of heat continues to the Arctic along the northern Spitsbergen (a reference temperature of 1°C) [Fahrbach, 2006; Rudels *et al.*, 2013; Schauer and Beszczynska-Möller, 2009; Schauer *et al.*, 2008]. This heat flux was found to increase since the 1980s [Dickson *et al.*, 2008].

During the recent decades, the time-series of the AW temperature in the Fram Strait and the Barents Sea Opening show a prominent long-term positive trend in the AW core temperature (around 1°C per decade in the WSC) [Schauer *et al.*, 2008], as well as interannual fluctuations with the characteristic periods of 5–6, 8–10 years [Bashmachnikov *et al.*, 2018; Muilwijk *et al.*, 2018; Skagseth *et al.*, 2008; Vesman *et al.*, 2017].

In this paper we analyze the space-time variability in the advective heat fluxes along the AW pathways into the Arctic. The main motivation of this work was to understand to what extent the anomalies of the oceanic heat flux, entering the Nordic Seas from the south, are conducted into the Arctic. This shows whether the observations at the southern transects (i.e., Svinøy) are representative for evaluation of the variability of the ocean heat advection to the Arctic on the interannual time scales. We also aim to investigate mechanisms behind a possible coherence loss along the AW path.

2. Data and Methods

2.1. ARMOR3D dataset

The 3D multi-observations of water temperature (T), salinity (S) and current speed (U , V) dataset (ARMOR3D), used in this study, is a collection of global gridded monthly 3D fields of temperature, salinity and geostrophic currents based on in situ and satellite observations. ARMOR3D gridded data have a spatial resolution of $0.25^{\circ} \times 0.25^{\circ}$. The data are available from 1993 through the web portal of Copernicus Marine Environment Monitoring Service [Verbrugge *et al.*, 2017]. Joint analysis of satellite (sea-level and sea surface temperature (SST) anomalies) and sub-satellite historical data through a multiple linear regression provides temperature and salinity values on a regular grid at different depth levels. These “synthetic” temperature and salinity profiles are combined with historical data in the optimal interpolation procedure to obtain the final monthly 3D thermohaline fields [Guinehut *et al.*, 2004, 2012]. Geostrophic currents are calculated by

extrapolating the sea-surface altimetry currents downwards using the thermohaline fields of the previous step and the thermal wind equations [Mulet *et al.*, 2012].

2.2. Mooring data

To validate the volume and heat fluxes derived from ARMOR3D, data from the moorings deployed in the Fram Strait by Alfred Wegener Institute [Beszczynska-Möller *et al.*, 2012, 2015] were used. The dataset consists of the temperature, salinity and currents speed information from 10 moorings stations deployed along 78.8°N from 8.70°E to 2.10°W during 1997–2011. The datasets are available online from PANGEA database [Beszczynska-Möller *et al.*, 2015]. Available precalculated oceanic heat fluxes from “North Atlantic Climate: Predictability of the climate in the North Atlantic/European sector” (NACLIM) project for the Hornbanki station located at 66.50°N 21.30°W [Jónsson and Valdimarsson, 2012] were also used for an additional validation of ARMOR3D dataset in the Denmark Strait.

2.3. Atmospheric data

The ocean–atmosphere heat exchange, as well as the short/long-wave radiation balance is derived from the ERA–Interim reanalysis [Dee *et al.*, 2011] distributed by the European Centre for Medium-range Weather Forecasts (ECMWF). Turbulent heat fluxes across the upper boundary, i.e., to/from the atmosphere, were calculated using the Coupled Ocean–Atmosphere Response Experiment (COARE) 3.5 algorithm. COARE 3.5, a modified version of the COARE 3.0 algorithm [Fairall *et al.*, 2003], is based on data from several experiments: the Climate Variability and Predictability (CLIVAR) and Mode Water Dynamics (CLIMOD), Marine Boundary Layer (MBL) and Coupled Boundary Layer Air–Sea Transfer (CBLAST) [Edson *et al.*, 2013].

2.4. Atmosphere circulation indexes

The North Atlantic Oscillation (NAO), Arctic Oscillation (AO) and East Atlantic (EA) indices were obtained from the NOAA National Weather Service Climate Prediction Center. The statistical links between the oceanic heat transport and the typical atmospheric pressure patterns, characterized by these indices, were estimated (see section 3.2).

In 1933, G. Y. Vangengeim suggested a set of indices characterizing atmospheric circulation. He introduced the concept of an elementary synoptic process [Barashkova *et al.*, 2015; Huth *et al.*, 2008; Vangengeim, 1933]. An elementary synoptic process is understood as the process during which, within the Atlantic-European sector, the geographic distribution of the sign of sea-surface atmospheric pressure anomalies and the directions of the main air transport patterns are preserved. Elementary synoptic processes can be generalized in three main types of the atmospheric circulation: the western (W), the eastern (E) and meridional (C) [Girs and Kondratovich, 1978; Prokhorova *et al.*]. For type W, the zonal component of the atmospheric circulation at mid-latitudes is strengthened and the meridional one is weakened. This circulation type leads to a significant reduction in the air exchange between the tropics and high latitudes. For type C, the Icelandic and Aleutian Lows are practically nonexistent due to a development of a high-pressure anomaly over the north Atlantic, similar to the so called Atlantic Ridge pattern. Further east, the Siberian Anticyclone strengthens and becomes connected with the Polar Anticyclone. Similar to type C, type E features strong meandering of the mid-latitude jet, but the high and low-pressure anomalies change sign. Thus, for type E, the Icelandic Low is well developed and the stationary anticyclone is observed over Europe and America – similar to the Scandinavian Ridge pattern [Bezuglova and Zinchenko, 2009]. Vangengeim – Giers classification helps to highlight variations of the wind patterns over the study region, only partly captured by the NAO and EA atmospheric indices. A more detailed description of these indexes is given in the Supplementary materials.

The Atlantic Multidecadal Oscillation (AMO) index, shaping the long-term variability of water temperature in the tropical to mid-latitude North Atlantic, i.e., the temperature of

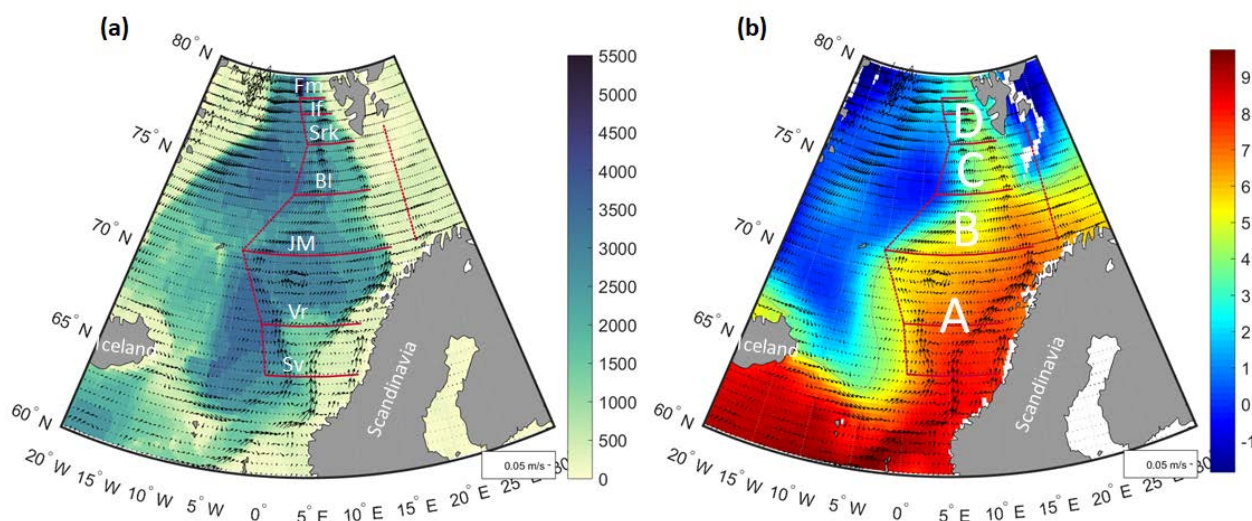


Figure 2. Transects used for the calculation of the oceanic heat fluxes and areas for calculations of the vertical heat fluxes (A–D). (a) represents the bathymetry (m), (b) – mean water temperature on 50 m ($^{\circ}\text{C}$). Black arrows indicate the mean currents at 50 m. The sections: Sv – Svinøy, Vr – Vøring, JM – Jan Mayen, BI – Bear Island, Srk – Sørkapp, If – Isfjord, Fm – Fram; the areas: A – from Svinøy to Jan Mayen, B – From Jan Mayen to Bear Island, C – from Bear Island to Sørkapp, D – from Sørkapp to Fram.

the waters entering the Nordic Seas, was also downloaded from NOAA National Weather Service Climate Prediction Center.

2.5. The study region

The positions of the transects used for the estimates of the meridional oceanic heat advection are presented in Figure 2. The sections were drawn to be approximately perpendicular to the direction of the mean currents, trapped by the continental slope and underwater ridges. The continental shelf was assumed as the eastern boundary for most of the sections. The western limits correspond to the points of the meridional transects with the minimum velocity of the NwAFC, just before the sign of the mean meridional flow is reversed (Figure 2). This accounts for the northwards transport, but minimizes the effects of the return flows on the results.

Some minor variations in the absolute values of the heat fluxes, when varying the eastern and western limits, are observed in the seasonal and interannual variability of the heat fluxes. However, the character of the variability remains unchanged (see example in Figure 3).

The heat fluxes through the western boundaries of the regions are most challenging to calculate with a sufficient precision. The instability of the NwAFC, a relatively large (monthly) period of data averaging, the medium resolution of the available data, and unaccounted ageostrophic component can lead to a significant change in the integral flux through the section even with a relatively small change in the position of the transects. Nevertheless, the trends and the interannual variability patterns are preserved (Figure 3). These uncertainties are further discussed when estimating the uncertainties of ocean heat convergence in the selected subregions: A (between the Svinøy and Jan Mayen transects); B (between the Jan Mayen and Bear Island transects); C (between the Bear Island and Sørkapp transects); D (between the Sørkapp and Fram strait transects). More examples for different positions of the transects and variation of the reference temperature are presented in the Supplementary materials (Figure A1).

Over the areas of the subregions A–D, the integral ocean-atmosphere and radiative heat-fluxes were also estimated.

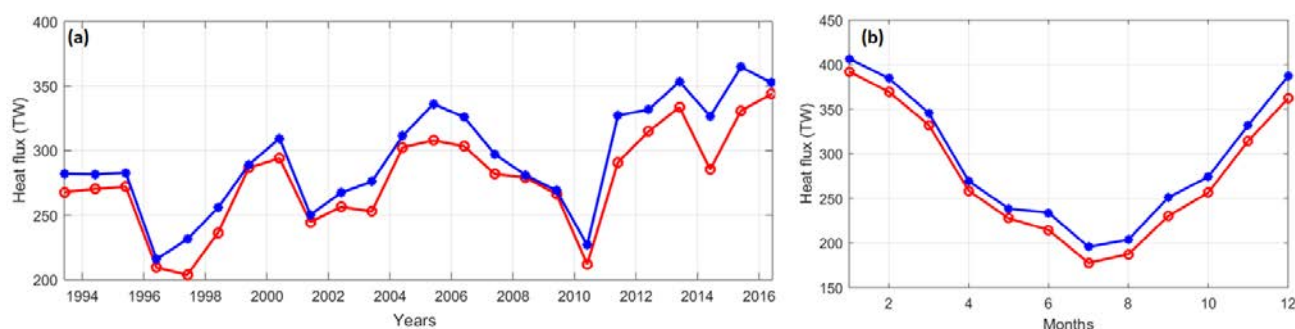


Figure 3. a – interannual and b – seasonal variability of the heat fluxes in the AW layer (ref $T = 0^{\circ}\text{C}$) across the Jan Mayen section computed for different positions of the western and the eastern boundaries of the study region: blue – the section extends from the Scandinavian coast to the Jan Mayen island, red – the section starts at the Scandinavian shelf break goes west up to the western edge of the NwAFC jet (estimated as the first minimum of the modulus of the current velocity west of the jet, as it is shown in Figure 2).

2.6. Advective heat fluxes

Total oceanic heat flux through the transect (Q) is computed by integrating the heat flux values in the grid points (1):

$$Q(t) = \rho_0 C_p \iint (T(x, z, t) - T_{\text{ref}}) V(x, z, t) dx dz, \quad (1)$$

where $\rho_0 = 1030 \text{ kg/m}^3$ is the mean sea water density; $C_p = 3900 \text{ J/(kg }^{\circ}\text{C)}$ is the specific heat of water; T is the sea water temperature in each grid-point and on each depth level, T_{ref} is the reference temperature, V is the current velocity perpendicular to the transect. The integration is done along the full length of the section and from the sea-surface to the lower boundary of the AW.

When comparing the values of the heat fluxes provided by various authors [Skagseth et al., 2008; Smedsrud et al., 2013], it is necessary to take into account different choices of the reference temperature. There is no justified algorithm for selection of the reference temperature [Schauer and Beszczynska-Möller, 2009]. Here as the “reference temperature” we use $T_{\text{ref}} = 0^{\circ}\text{C}$, as in most of the previous studies in the region [Bacon et al., 2015; Hansen et al., 2008; Skagseth et al., 2008; Smedsrud et al., 2013; Walczowski, 2014]. Experiments show that different choice of the reference temperature have only minor effects on the interannual variations, which are of primary interest here. In this study we integrate the advective heat fluxes over the Atlantic Water layer (see Figure A1 in the Appendix A).

2.7. The Atlantic Water in the eastern Nordic Seas

Although the term “Atlantic Water” is widely used in a number of studies, there is no common criterion for definition of the AW in the Nordic Seas. Depending on the goals and on a research area, different criteria (based on temperature, salinity, potential density or other parameters) and different threshold values are used (Table 1).

In this study, following Furevik et al. [2007], we limit the AW from below with a potential density threshold, which largely corresponds to the temperature and salinity thresholds, used in alternative studies. Furevik et al. [2007] give a rather broad range of the threshold values, increasing northwards. This is due to the densification of the AW as it moves north [Latarius and Quadfasel, 2016]. To select the optimal threshold density values, the time-mean depths of various isopycnals from this range were overlaid on the vertical distribution of temperature and salinity along the transects (Figure 4). This allows testing the criteria against temperature and salinity thresholds used for defining the AW in different areas of the Nordic Seas (Table 1). From our analysis, 27.8 kg/m^3 isopycnal was selected as the lower boundary of the AW at the Svinøy section, 27.85 kg/m^3 – at the Vøring section,

Table 1. Criteria used for definition of the AW in different studies

Region	Criteria of the AW (<i>T</i> is temperature, <i>S</i> is salinity)	Reference
Nordic Seas as a whole (based on Svinøy section)	$T > 1^{\circ}\text{C}$	[Mork and Blindheim, 2000]
	$T > 5^{\circ}\text{C}, S > 35$	[Orvik et al., 2001]
	AW temperature = mean temperature in a layer of 70–500 meters, current direction to the north	[Muilwijk et al., 2018]
	$S > 35$	[Mork and Skagseth, 2010]
Svinøy section (or southern boundary of Nordic Seas)	$T > 55^{\circ}\text{C}, S > 35$	[Wekerle et al., 2017]
	$T > 7\text{--}10^{\circ}\text{C}$	[Beszczynska-Möller et al., 2015]
	$T > 7\text{--}8^{\circ}\text{C}, S > 35.2$	[Walczowski, 2014]
From Svinøy section to 79°N	Potential density = $27.5\text{--}28.0\text{ kg/m}^3$	[Furevik et al., 2007]
Svinøy, Gimsoy, Sørkapp (layer 50–200 m)	$T = 2.5\text{--}9.5^{\circ}\text{C}, S = 34.9\text{--}35.3$	[Furevik et al., 2007]
Barents Sea opening	$T > 5^{\circ}\text{C}, S > 35$	[Wekerle et al., 2017]
	$T > 6\text{--}6.5^{\circ}\text{C}$	[Beszczynska-Möller et al., 2015]
Gimsoy section	$T = 6\text{--}6.5^{\circ}\text{C}, S > 35.15$	[Walczowski, 2014]
West-Spitsbergen current	$T > 2^{\circ}\text{C}, S > 34.88$	[Cokelet et al., 2008]
Fram Strait	$T > 2^{\circ}\text{C}, S > 35$	[Wekerle et al., 2017]
	$T > 3\text{--}3.5^{\circ}\text{C}$	[Beszczynska-Möller et al., 2015]
	$T > 2^{\circ}\text{C}, S > 34.95$	[Walczowski, 2014]
Arctic Ocean	$T > 0^{\circ}\text{C}$	[Polyakov et al., 2017]

27.9 kg/m^3 – at the Jan Mayen section, 27.95 kg/m^3 – at the Bear Island section, 28 kg/m^3 – at the Sørkapp, Isfjord and Fram sections. In between the sections, the isopycnals from the southern section were used to mark the lower boundary of the AW.

2.8. Vertical mixing

The vertical turbulent heat fluxes through the base of the AW layer are estimated as:

$$Q_{\text{vert}} = C_p \rho_0 K_z \Delta T / \Delta z, \quad (2)$$

where ΔT is the temperature differences between the lower boundary of the AW and the first level below the selected AW limit; Δz is the vertical distance at which the ΔT drop is observed (for the data used Δz was typically 100 m). Two methods were used for obtaining K_z values: (1) $K_z = \text{const} = 10^{-5}\text{ m}^2/\text{s}$ [Fer et al., 2018] and (2) K_z was estimated through the Richardson number [Timmermann and Beckmann, 2004], which combines Pacanowski and Philander [1981] parameterization with a diagnostic scheme using the Monin – Obukhov length.

In the second case [Pacanowski and Philander, 1981], the diffusion coefficient is estimated as:

$$K_z = \frac{k^{uv}}{1 + 5Ri} + k_b^{TS}, \quad (3)$$

where

$$k^{uv} = k_{\text{pp}}^{uv} + k_{\text{mo}}^{uv},$$

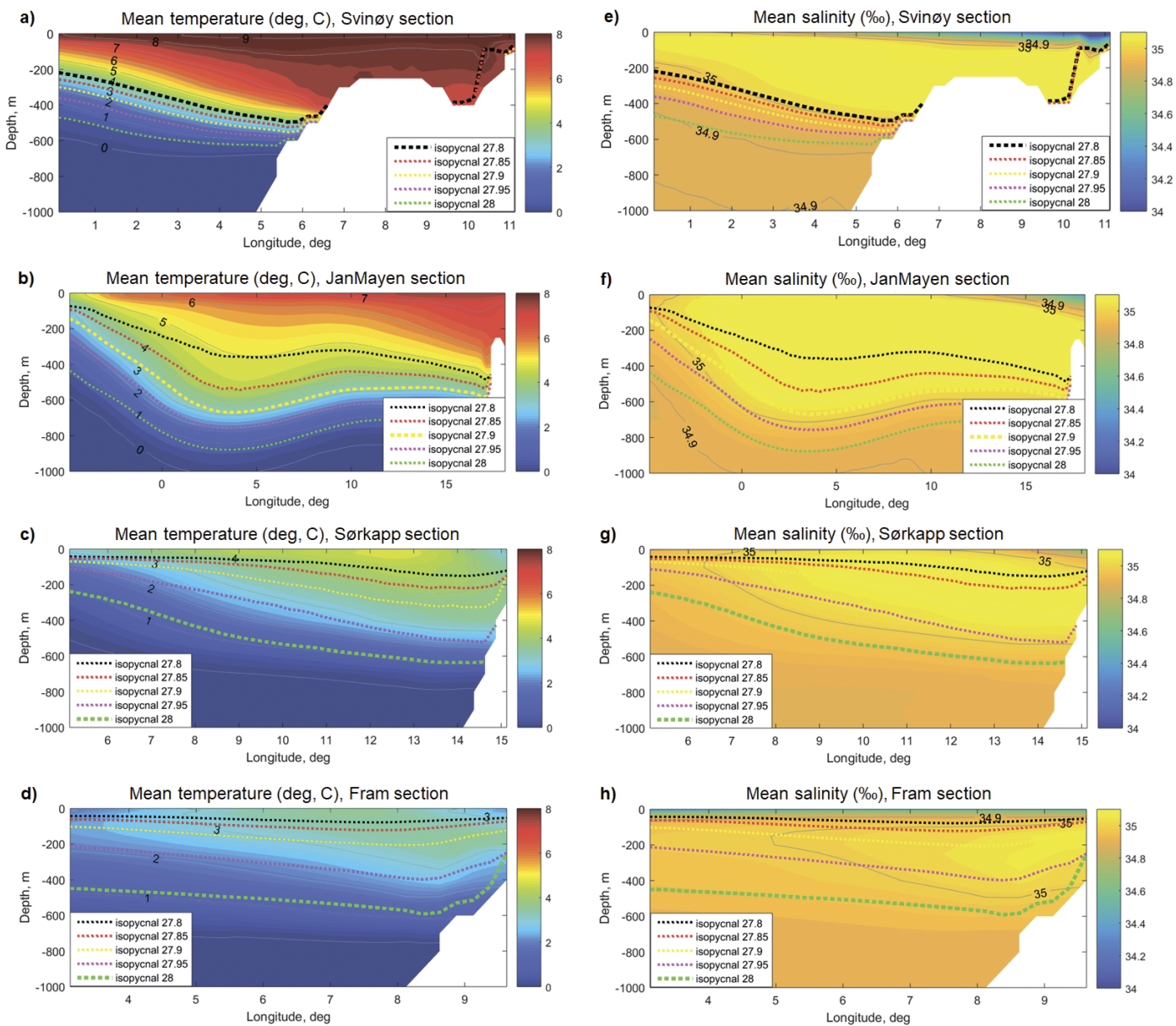


Figure 4. Temperature (left column) and salinity (right column) along the selected transects from the south to the north. a, b, c, d – temperature on Svinøy, Jan Mayen, Sørkapp and Fram sections accordingly; e, f, g, h – salinity on Svinøy, Jan Mayen, Sørkapp and Fram sections accordingly. Isopycnals of potential density 27.8 (black), 27.85 (red), 27.9 (yellow), 27.95 (magenta), 28 (green) are overlaid, thicker dashed line highlights isopycnal outlining the AW layer.

$$k_{pp}^{uv} = \frac{v_0}{(1 + 5Ri)^2} + k_b^{uv},$$

$v_0 = 0.01 \text{ m}^2/\text{s}$, $k_b^{uv} = 10^{-4} \text{ m}^2/\text{s}$, $k_b^{TS} = 10^{-4} \text{ m}^2/\text{s}$. The gravitational instability (convection) is accounted for by additional term [Timmermann and Beckmann, 2004]:

$$k_{mo}^{uv} = \begin{cases} 0.01 \text{ m}^2/\text{s}, & \text{for } |z| < \hat{h}' \\ 0 \text{ m}^2/\text{s}, & \text{for } |z| \geq \hat{h}' \end{cases},$$

where \hat{h}' is the vertical scale linked to the Monin – Obukhov length. In our study no convective mixing through the lower interface at around 500 m depth was registered, so we set $k_{mo}^{uv} = 0$.

Substituting all the coefficients to the (3), we obtain:

$$K_z = \frac{k^{uv}}{1 + 5Ri} + 10^{-5},$$

As currents in the ARMOR3D dataset are geostrophic, we calculate the Richardson number from the horizontal density gradients using the geostrophic relations:

$$Ri = \frac{N^2}{\left(\frac{dU}{dz}\right)^2 + \left(\frac{dV}{dz}\right)^2} = \frac{N^2}{R^2},$$

where $N = \sqrt{-\frac{g}{\rho_0} \frac{d\rho}{dz}}$ is the buoyancy frequency, $R = \frac{g \sqrt{\left(\frac{d\rho}{dy}\right)^2 + \left(\frac{d\rho}{dx}\right)^2}}{\rho_0 f}$ and f is the Coriolis parameter:

The K_z estimates using both methods were found to be very close to each other.

3. Results and discussion

3.1. Validation of ARMOR3D data

To validate the ARMOR3D estimates, we compare the statistical properties of available mooring observations in the Fram Strait (AWI F1–F10) with the data in the nearest grid-point of the ARMOR3D dataset. The first pre-processing steps include removal of outliers and monthly averaging of the data to cope with the ARMOR3D temporal resolution. Then the ARMOR3D and the moorings data are binned to 100 m vertical bins centered on the position of the available moored instruments (provided a certain inconsistency in the depths of the instruments after re-deployment of the moorings and the limited vertical resolution of ARMOR3D). Figure 5 shows an example of the time series of temperature, velocity and heat fluxes at the mooring F5 (located in the eastern Fram Strait 78.5°N and 6°E). The Taylor diagrams [Taylor, 2001] show that the temperature variability is well reproduced by the ARMOR3D dataset (the correlation coefficient is 0.6 for the annual mean values). On the other hand, the current velocity (and the heat flux) derived from ARMOR3D, shows a consistently lower absolute values (Figure 5). The monthly mean current velocities, derived from the mooring data, also show a significantly higher variability compared to the altimetry based ARMOR3D data. For annual mean U and V components, which are of the main interest for this study, correlations between the data-sets increase (in the presented example, from 0.5 to 0.7 and from 0.6 to 0.7, respectively). Removing long-term trends from the time series results in a slight decrease in the correlations for the cross-flow U component (to 0.4), while it does not change that for the along-flow V component and for water temperature. The meridional velocity component is along the direction of the geostrophic flow in the region. Therefore it is much better reproduced by the geostrophic ARMOR3D current. In the velocity component perpendicular to the bottom slope (V at this section) we may expect a strong ageostrophic component. Figure 5 shows the seasonal and the interannual variability of the oceanic heat fluxes are also reproduced in ARMOR3D with a reasonable accuracy (the correlation coefficient is 0.6), at least for the West Spitsbergen Current (mooring F5). Overall, in further analysis we may expect a higher accuracy of the heat fluxes across the zonal sections (currents across the sections are mostly along the topography and should be largely geostrophic), compared to the sections limiting the study sub-regions from the west (directed along the topography and presumably containing a strong ageostrophic component).

In the areas with the presence of the drifting ice (the East Greenland Current) and at deeper water levels, the performance of ARMOR3D in comparison to the mooring data naturally decreases. This is due to a degradation of the satellite altimetry data in the ice-covered areas and due to an error accumulation in the process of the downwards integration of the water density gradients, respectively. For the present study, focused on the upper 500-meter layer and in the regions with no winter ice cover, we consider the

ARMOR3D dataset to represent the interannual variability of the heat fluxes reasonably well (see Figure 5).

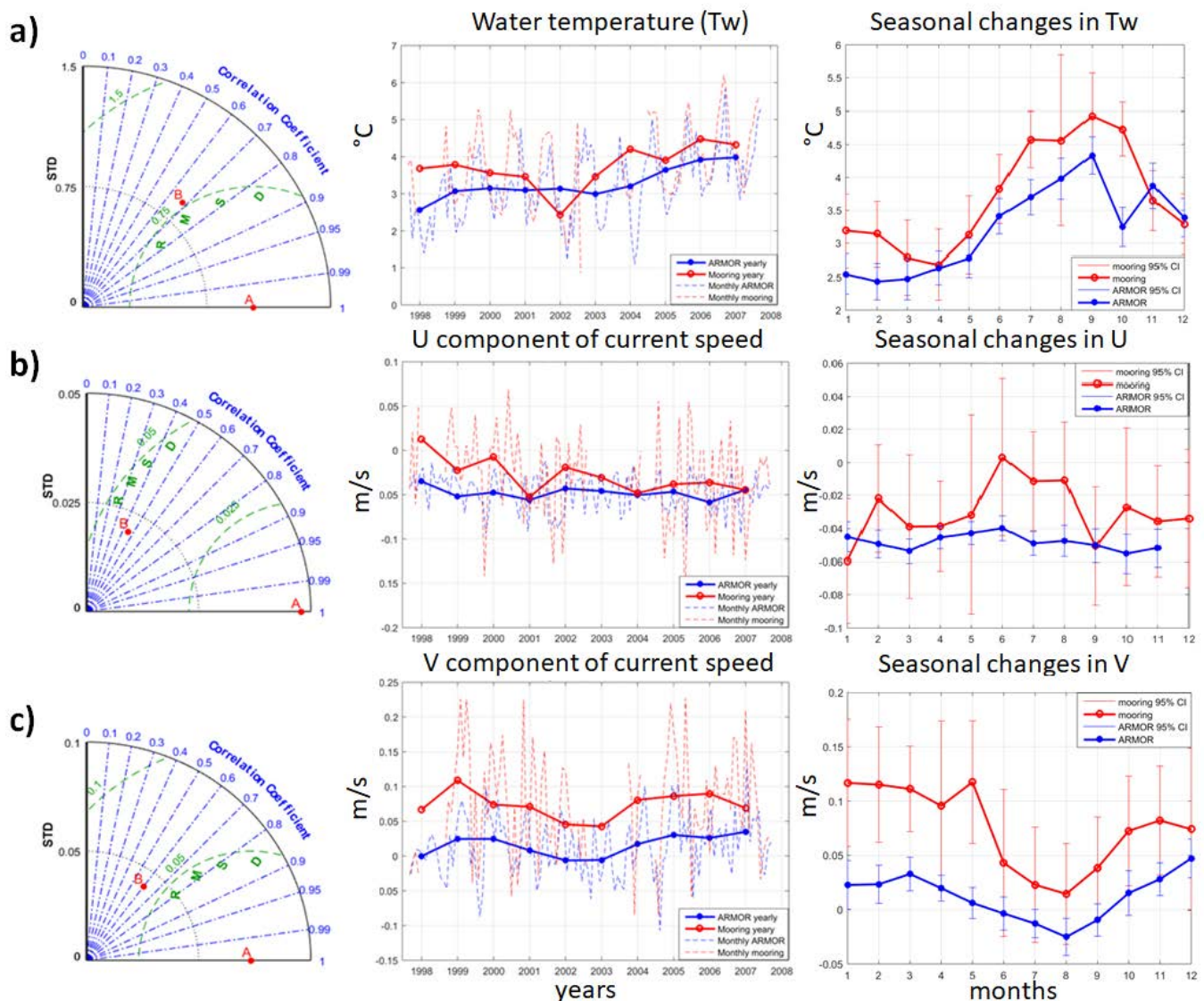


Figure 5. Validation of ARMOR-3D (blue) against in situ data at mooring F5 (red) located in the WSC at 78.5°N 6°E: a – water temperature (°C), b – zonal current velocity U (cm/s) and c – meridional current velocity V (cm/s). Left – Taylor diagrams (ARMOR-3D is point B, in situ – point A), center – data time series, right – seasonal cycles. Data are averaged in 50–150 m layer.

3.2. Temporal variability of heat fluxes along the NwAC

The Svinøy section is one of the main sites where the AW inflow into the Nordic Seas is monitored continuously [Orvik and Nüiler, 2002; Raj et al., 2018]. The heat advection across this section integrates three main cores of the warm water coming from the south: the coastal branch at around 10°E (the NwACC) that carries a fresher water of the Baltic origin, further affected by the freshwater runoff off the Norwegian coast [Gascard and Mork, 2008], the slope branch between 5 and 6°E (the NwASC) and the polar front branch between 2 and 3°E (the NwAFC). Our analysis shows that the largest mean heat flux over the study period is directed northward along with the NwASC. From the Svinøy (the heat advection is 406 TW) to Jan Mayen sections (the heat advection is 341 TW) the oceanic advection of heat decreases by about 1/3. This is consistent with the observed significant heat loss of the

NwASC and NwAFC towards the interior of the Lofoten Basin, the main heat reservoir in the Nordic seas [Bashmachnikov *et al.*, 2023; Björk *et al.*, 2001; Bosse *et al.*, 2018]. The NwASC heat loss mainly goes through generation of eddies drifting west, while that of the NwAFC also results from a recirculation pattern in the southern part of the Lofoten Basin [Raj *et al.*, 2020]. Mean integrated heat fluxes have more or less similar seasonal patterns at all the transects and for all the years during the study period: the heat flux decreases in summer and increases in winter, which is in line with the previous results on the heat transport in this area [Mork and Skagseth, 2010; Skagseth *et al.*, 2004, 2008]. This seasonal cycle is regulated by the seasonal variability of the current velocity (higher in winter). The winter maximum of the NwASC is explained by a higher sea-level gradient caused by an increased Ekman pumping associated with stronger northward-blowing winds along the Scandinavian coast [Mork and Skagseth, 2010; Skagseth *et al.*, 2008]. Further in this paper we extend the analysis by Chafik *et al.* [2016], who studied the consistency of interannual variations of the NwASC along the Vøring plateau, by analyzing the interannual variations of heat fluxes further north, up to the Fram Strait.

Besides 406 TW which enters the Norwegian Sea across the Svinøy section on average over the study period (1993–2017), another 132 TW enters the study region from the west, across a deep Aegir Ridge and the Jan Mayen Fracture Zone (the western boundary of region A shown in Figure 6). These western boundary ridges (as well as Mohn-Knipovich ridges further north) do not rise above 1500–2000 m depth levels, far below the lower AW limit. The dynamic boundary of the topographically steered NwAFC, limiting the study region from the west, is a subject of a relatively intensive cross-frontal exchange [Raj *et al.*, 2019]. Only half of the overall incoming heat crosses the Jan Mayen section (~341 TW) at the northern boundary of region A. From this heat flux, about 89 TW enters the Barents Sea through the Barents Sea Opening, while 131 TW continues north across the Bear Island section (northern boundary of region B). Only 54 TW, around 1/10 of the heat entering the Lofoten Basin, reaches the Fram section (the northern boundary of region D). The heat fluxes across the western boundary of the regions B–D are comparatively small and highly variable. In region D, the westwards heat flux of about 3 TW represents a southern branch the AW southwestwards recirculation into the western Greenland Sea [von Appen *et al.*, 2015]. A significant amount of heat is lost due to the vertical mixing across the AW boundary (Figure 6), being the strongest in the Lofoten Basin, where convection across the AW lower boundary is episodically observed [Bosse *et al.*, 2018; Fedorov *et al.*, 2019]. The advected heat, as well as other main components of the heat balance in regions A–D, are schematically shown in Figure 6. The imbalances obtained account for 10–20% of the incoming heat advection and reflect the observed warming of the AW in the Norwegian Sea.

To evaluate the robustness of the results above, several sensitivity experiments were conducted. First, in addition to the estimates from ERA-Interim reanalysis, heat fluxes across the ocean surface were also estimated using alternative reanalyses: ERA5, ASR, OAFlux. The results show practically the same interannual variability of the integral heat fluxes over the study regions (see Figure A2). Second, the values of the oceanic heat advection may depend on the position of the transects (sometimes rather small changes may affect the resulting values), as well as on the reference temperature. It was shown that the variations in the section positions, as well as of T_{ref} (the typically used values $T_{\text{ref}} = -1, -0.5$ and 0°C were tested), do affect the values of the heat balances of the study sub-regions. However, practically no change was found neither in the decadal tendencies nor in the interannual variations of the ocean heat advection, the main focuses of this study (see Figure A1). This goes well with the previous results by [Schauer and Beszczynska-Möller, 2009], who consider uncertainties in the oceanic heat fluxes resulting from the choice of the reference temperature and suggest treating the oceanic heat advection in terms of their variability, rather than relying on their absolute values.

The AW changes its properties on its way north through mixing with the surrounding water and the ocean-atmosphere exchange. Going at different rate, which vary in space and

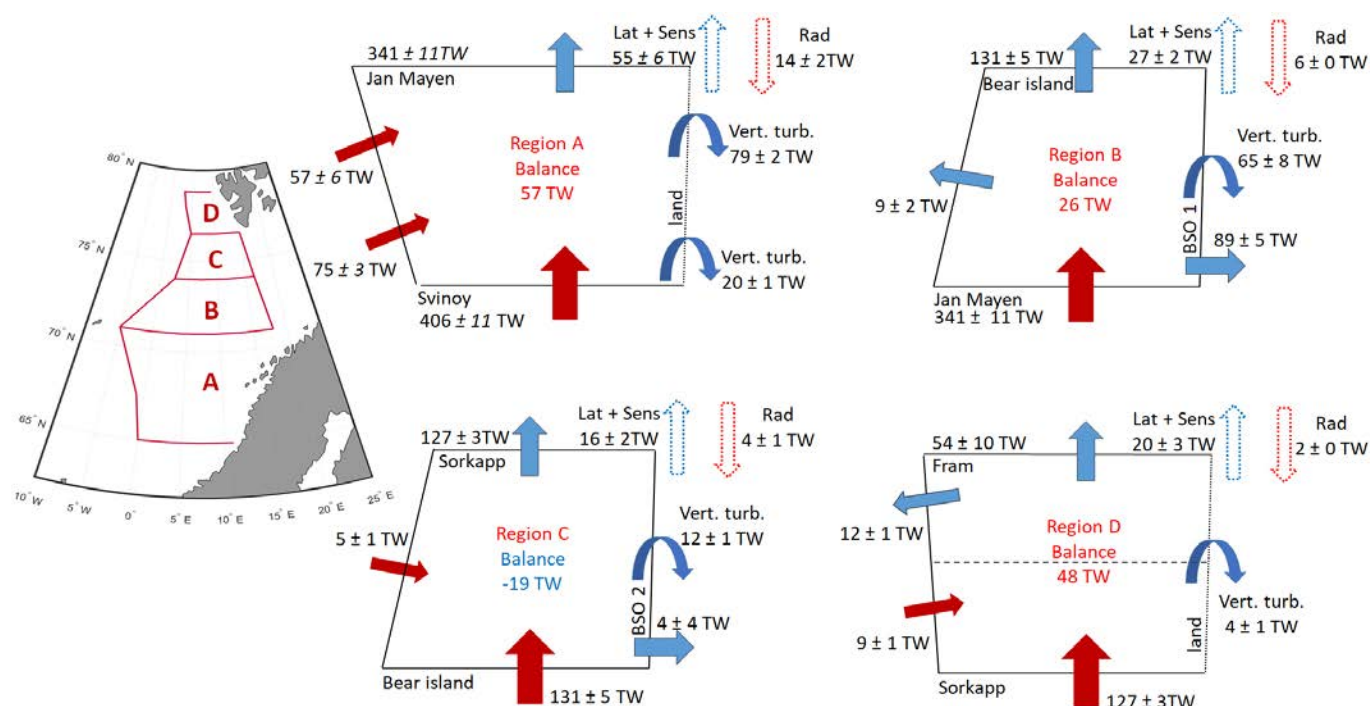


Figure 6. Components of the mean (1993–2017) heat balance for regions A–D. Filled red (blue) arrows represent the oceanic heat fluxes entering (leaving) the regions, dashed arrows represent latent and sensible heat fluxes from ocean to atmosphere (blue) and radiation balance of the ocean surface (red), curved arrow represents vertical turbulent heat flux. The heat fluxes are given together with \pm errors of the means (at the 95% confidence level).

time, these water mass transformations add to the variations in the current velocity and contribute to the loss of correlations of the advective heat fluxes crossing different transects (Figure 7). The correlations drop gradually with distance between the correlated transects. The correlations between the heat advection at the neighboring transects, separated by 200–300 km, is high (0.7–0.8). Similarly, Skagseth et al. [2008] found a coherence between the temperature and salinity variations at the Svinøy and the Sørkapp/BSO sections on the decadal time scales. Our results show that correlations between the sections in the Lofoten Basin and the transects further north drop to insignificant north of Sørkapp section. The correlation drop between the Svinøy and Sørkapp section might be affected by the 1-year period required for an anomaly to propagate from 63 to 76°N, given the mean propagation velocity of thermohaline anomalies of 3 cm/s [Walczowski, 2014]. However, the cross-correlation analysis with the seasonal cycle removed shows that the maximum correlations are at zero time lag (Figure A3), which suggests a simultaneous (though different) forcing at all sections on the interannual time scales.

After removing the trend in the deseasoned data, the cross-correlation between the southern sections (Svinøy to Jan Mayen) and the northern sections (Sørkapp to Fram) increases, while this procedure does not affect the correlation drop between Svinøy and Jan Mayen (Figure 7b). Thus, there are different patterns of the long-term variability in the southern and the northern set of sections, which affect the correlations (see also Figure 9a,b).

The results above suggest different mechanisms controlling heat transport of the NwAC across the southern and northern sections. Correlation analysis shows that only the heat fluxes across the southern sections show significant, though moderate (0.3–0.5), positive correlation with the NAO, AO and EA indices (Table 2). For the northern sections the correlations go to insignificant values (close to 0). Previously, Chafik et al. [2015] showed that NAO is not the driving mode for the AW flux through the Fram Strait, while the regional atmospheric circulation is the main driving factor. Also Skagseth et al. [2008] and

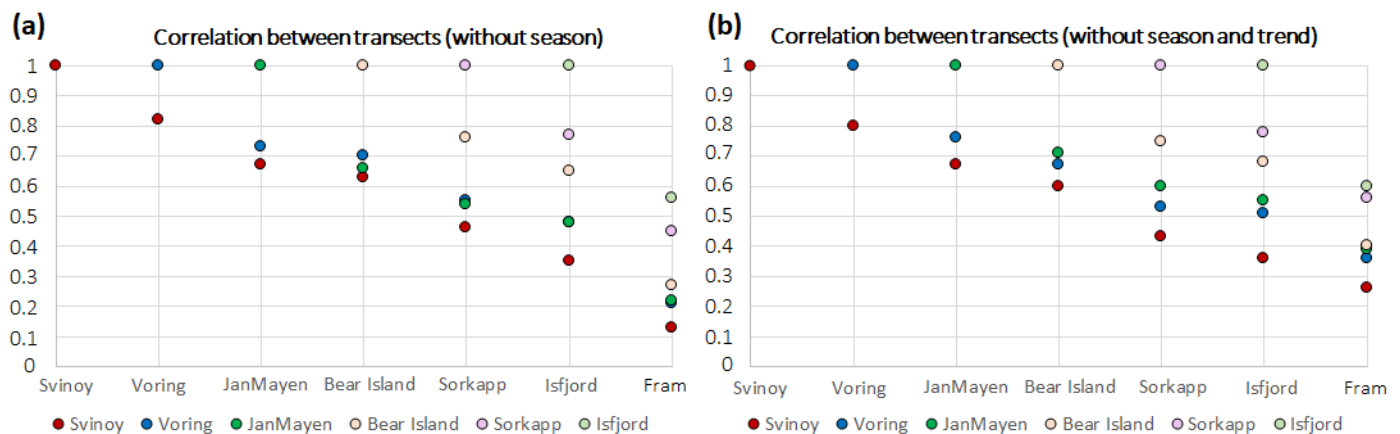


Figure 7. Correlation coefficients between monthly mean values of the heat flux across the selected transects (Figure 2a): a – the seasonal cycle is removed, b – the seasonal cycle and trend are removed.

Raj et al. [2018] suggest the NAO to be an important agent in modulating the AW transport along the southwestern Scandinavian coast, while Lien et al. [2013] have shown that the relative strengths of the branches of the AW along the western Spitsbergen and in the Barents Sea are strongly affected by a regional atmospheric circulation pattern over the Spitsbergen and the northwestern Barents Sea: a higher AW transport into the Barents Sea is accompanied by a lower transport through the Fram Strait see also Kalavichchi and Bashmachnikov [2021].

Table 2. Correlation coefficients between the oceanic heat advection across the selected transects and various atmospheric indices (bold – significant values at the 95% significance level)

	Svinøy	Vøring	Jan Mayen	Bear Island	Sørkapp	Fram
NAO	0.46	0.45	0.26	0.09	0.06	−0.02
AO	0.47	0.45	0.23	0.18	0.17	0.05
EA	0.39	0.34	0.18	0.13	−0.15	−0.26
AMO	0.13	0.23	0.33	0.21	0.09	0.06
E	−0.09	−0.02	−0.06	0.03	−0.14	−0.25
C	−0.46	−0.41	−0.29	−0.26	−0.33	−0.24
W	0.39	0.30	0.25	0.15	0.35	0.38

On the other hand, a consistent sign of the correlations between the advective heat fluxes at all sections and the weather types C and W was obtained (Table 2). Even though significant only for some northernmost and the southernmost sections, the correlation coefficients with the western weather type W remain all positive, while with the central weather type C remain all negative. This suggests a possible affect of the large-scale wind forcing pattern, responsible for the corresponding variations all along the NwAC.

Along with the sea-level drop/increase near the coast, which depends on the direction and intensity of the along-coast wind component, we consider the convergence/divergence of the Ekman flux in the open ocean (Ekman pumping), which is proportional to the wind stress curl.

In the first case, the horizontal divergence in the Ekman layer near the coast can be estimated as:

$$\text{div}V = \frac{\tau_l}{\rho f L}, \quad (4)$$

where τ is the wind stress curl, τ_l is the wind stress curl component along the coast, c is the mean water density, f is the Coriolis parameter and L is the distance from the coast, V – vertically averaged horizontal velocity in the Ekman layer.

In the second case the divergence of Ekman fluxes at the sea-surface can be computed as:

$$\text{div} V = -\frac{1}{\rho f} \text{rot}(\tau). \quad (5)$$

In this study we are interested in the anomalies of the horizontal divergence (which by continuity means the anomalies of the vertical velocity) relative to the climatic mean wind fields associated with weather types W, C, E (Figure 8). Acceleration/deceleration of the currents are formed by changes in the sea-level gradients across the axes of the branches of the Norwegian Current, forced by the wind fields characteristic for a particular weather type. In Figure 8, changes in the sea-level for each of the weather types relative the climatic mean state are presented as the vertical velocity anomalies, the gradients of which are of the main interest below.

Along the Norwegian coast, the acceleration of the along-shore branch of the NwASC due to the sea-level build-up (forced by the southwesterly winds, (4) is expected for weather types E (Figure 8c) and W (Figure 8a), but not for C (Figure 8b). For type W, the anticyclonic wind-stress curl also results in an anomaly of the water convergence by Ekman pumping (5) along the Norwegian shelf and over the Vøring plateau. The same is observed along the continental slope west of the Barents Sea Opening. This further increases the sea-level build-up east of the NwASC all the way to 75°N (5), maintaining a higher current velocity and a stronger heat advection. The opposite tendency in the Ekman convergence (5) is observed for types E and C. For type E, the Ekman convergence (5) diminishes the effect of the near coast sea-level build-up resulting from Eq. (4), while for type C it enhances the negative near-coast sea-level anomalies resulting from Eq. (4).

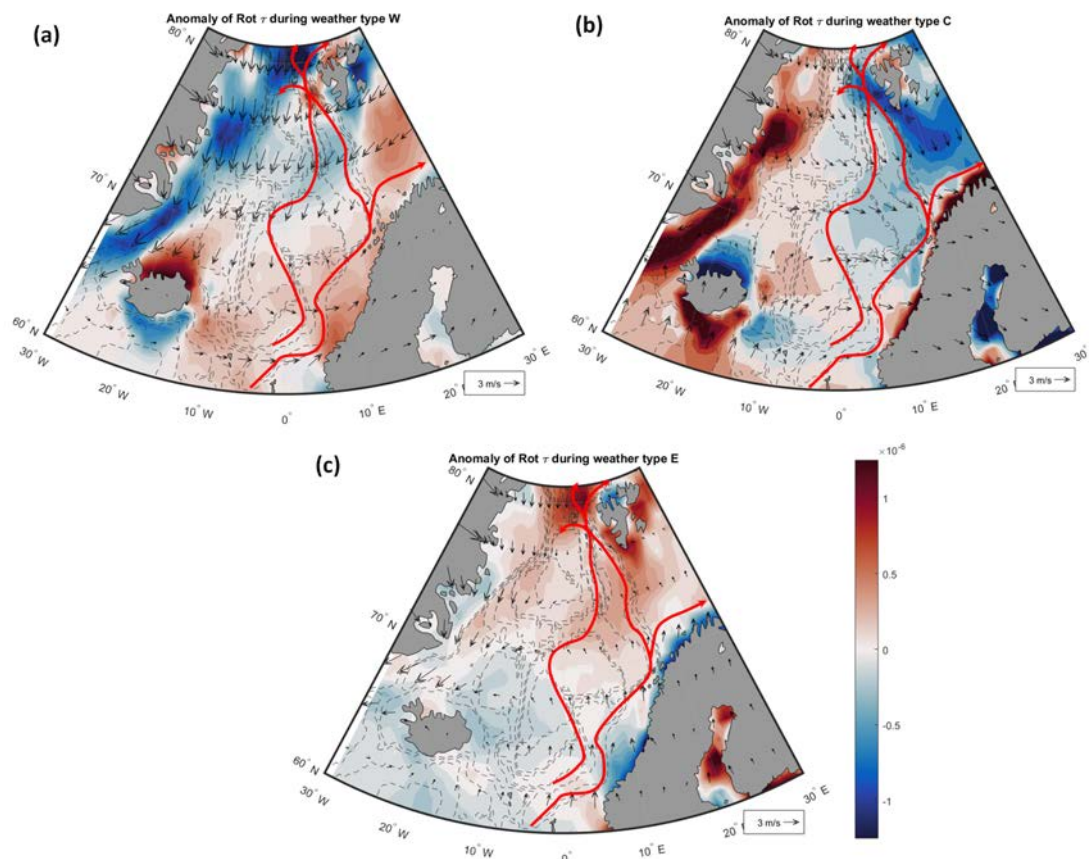


Figure 8. Anomalies of the wind stress curl (red – increase of the sea level, blue – decrease of the sea level, m/s), dominant wind patterns (vectors) over the North Atlantic associated with circulation types: a – W, b – C and c – E, dashed lines – bathymetry, red arrows – AW pass.

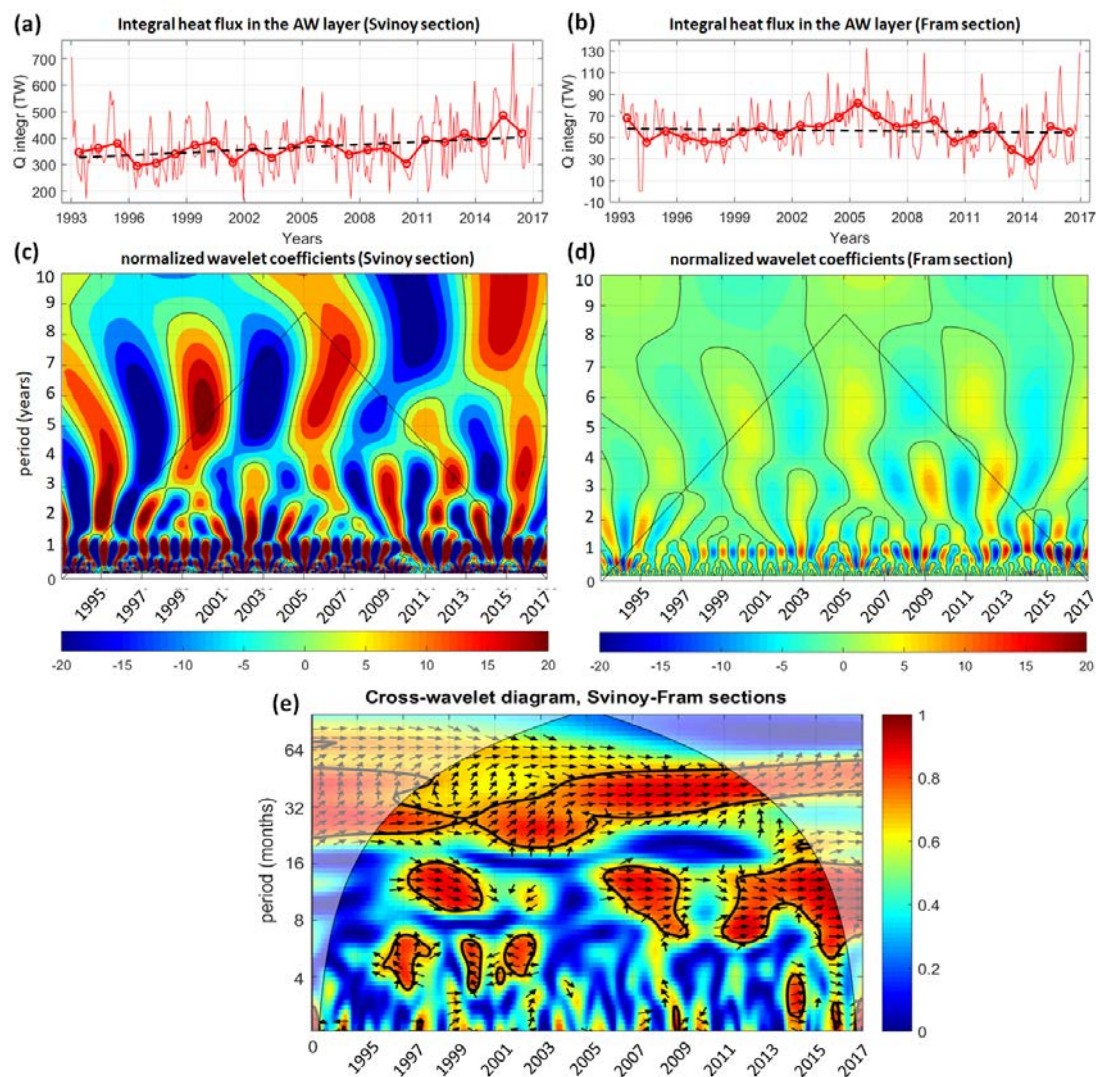


Figure 9. Time series (a, b) and wavelet diagrams (c, d) of interannual variations of heat advection across the Svinøy section (a, c) and across the Fram section (b, d), e – cross-wavelet diagram between the Svinøy and Fram sections.

Besides, type C favors a stronger warm AW outflow into the Barents Sea, while the opposite situation is observed for type W and E.

West of Spitsbergen, the wind-stress curl of the weather type W maintains an increase in transport of the NwAFC and WSC at 79°N, while further south an acceleration of the NwASC may be compensated by a deceleration of the WSC. For weather type E, an acceleration along the southern part of the island is accompanied by a deceleration further north. For weather type C a clear deceleration of both, the WSC and NwASC is governed by a northeastwards increase of the negative vertical velocity forced by Ekman pumping.

In summary, the analysis above suggests that the Ekman pumping forced by the wind stress curl, together with a near-coast sea-level build-up (mostly along the Norwegian coast), should increase the northward current velocity practically along all its path through the Nordic Seas for weather type W and decrease – for weather type C. For weather type E the current accelerations and the decelerations alternate downstream along the NwAC. For this weather type, characterized by gentle winds and a relatively small variation of the Ekman pumping anomalies over the Nordic Seas, we do not expect a consistent increase or decrease of the AW transport along its northward pathways.

From 1993 to 2017 there is no pronounced positive or negative long-term trend (Figure 9 a,b) in the heat flux across most of the sections (apart from the BSO section, where the heat advection consistently grows with time during this period – not shown, see *Kalavichchi and Bashmachnikov* [2019]). At Svinøy section there is a certain tendency for oceanic heat advection to grow, the most pronounced since 2010. This is in line with the recent AW warming of the upper Norwegian Sea since 2010–2011 derived from Argo profiles [*Mork et al.*, 2019]. However, the heat advection across the Fram section increases only in the beginning of the 2000s. Since 2005 it started decreasing, with some recovery in 2016–2017. Overall, no significant long-term trend is noted during the study period. Thus, despite the general increase in the water temperature in the southern part of the region, the northern sections do not demonstrate a positive trend in the heat advection during the latest decades. This is one of the factors reducing the correlations.

To detect hidden periodicities in the heat advection across the selected transects, the wavelet analysis with the Morlet mother wavelets is applied [*Torrence and Compo*, 1998]. In all the transects the dominating periodicities of 3 years and of 5–6 years can be detected (Figure 9c,d, see also Figure A4). The wavelet amplitudes decrease northwards, along with the decrease of the intensity of the mean ocean heat advection. The cross-wavelet diagrams show a high coherence of heat fluxes across the Svinøy and Fram sections at 2–5 years, the variability being in phase. This suggests that on intra-decadal time scales there is a certain coherence in the oceanic heat advection along the NwAC. At the same time, the amplitude of the 5 year oscillation drops by 50% from the Svinøy to Bear Island sections and by another 60% from the Bear Island to Fram sections, while the amplitude of the 3 year oscillation drops by 40% from the Svinøy to Bear Island sections and only by 8% from the Bear Island to Fram sections. We further note that for weather types W and C we also observed the dominating oscillations at 2–3 and 5–7 year periods, which further supports a suggested link between the oceanic heat advection along the NwAC and W and C weather patterns.

4. Conclusions

The present analysis suggests a certain consistency of the heat fluxes along the AW path through the Nordic Seas. At all sections 3 and 5–6 year oscillations dominate in the short-term interannual variability. High wavelet coherence of the heat advection across the southern and northern sections is observed at these time scales. The coherent reaction of the advection intensity all along the AW pathways from the Svinøy to Fram sections at the time scales above can be linked to the coherent atmospheric forcing, as a result of a varying relative annual frequency of C and W weather types, as the indices of these weather types show the same periodicity. The link between the atmospheric patterns and the ocean advection is suggested to be a reaction on the weather conditions of a spatial structure of Ekman pumping. In this study we took into account the sea-level variations resulting from a change in the wind stress curl, as well as in the sea-level build-up near a coast. These processes suggest an increase in the heat advection along the whole path of the NwAC for weather type W and a decrease for weather type C. It is reflected also in the opposite sign of correlations of the annual frequencies of these weather types with the intensity of heat advection all along the path of the AW.

Beyond the similarity above, there are also notable differences in the interannual variability in the intensity of heat advection between the southern and northern sections. This is reflected in a drop of correlations between the southernmost section and those further north, particularly strong when crossing the Lofoten Basin (between the Svinøy and Jan Mayen sections) and between the Bear Island and Sorkapp sections. The drops from the southern and northern groups of sections are partly due to the opposite long-term trends after the mid 2000s in these different groups (Figure 9a–b). One of the reasons for this different behavior may be a dependence of the heat advection on different atmospheric patterns. Thus, advection across the southern sections are linked to the NAO-type pattern, which practically does not influence the northern sections (Table 2, see also *Raj et al.* [2018]).

In turn, the heat fluxes across the northern sections should respond to a variability of the local cyclonic wind pattern centered in the north-western Barents Sea [Chafik *et al.*, 2015; Lien *et al.*, 2013]. Also a drop of correlation should be a result of a differential damping of the dominating interannual oscillations of the heat advection downstream of the NwAC: the 5-year oscillations are damped much more effectively than the 3-year ones. The observed damping might be linked to variation in the intensity of the heat extraction by eddies generated at the NwASC [Bashmachnikov *et al.*, 2023].

The oceanic heat inflow in the selected areas, bounded by the selected transects (regions A–D), is largely balanced by the heat release to the atmosphere and by vertical mixing with the cold intermediate water from the Greenland Sea. The first process dominates in the northern regions (west of Spitsbergen), while the second becomes important in the Lofoten Basin, where a relatively deep convection is observed. The imbalances between the main heat fluxes range from 10 to 20% of the heat advected into region A from the south, across the Svinøy section. This results in an observed warming of the AW layer in the Nordic Seas during recent decades. Eddy heat fluxes from the Norwegian to Greenland Sea, not estimated in the present study, is also a part of these imbalances [Bashmachnikov *et al.*, 2020, 2023; Raj *et al.*, 2020]. On the other hand, validation of the ARMOR3D dataset against data from mooring show that the oceanic heat advection derived from ARMOR3D may contain some biases (Figure 5), on particular at the meridional sections, add to the imbalances. Sensitivity experiments also showed that the choice of the reference temperature can also influence the results. However, these drawbacks of the dataset used affect the absolute values of the oceanic heat advection, but the dataset is proved to reproduce well the interannual variability of the heat advection, which is the main focus of this study.

Acknowledgments. The work of A. V. Vesman was done in frame of the topic 5.1.4 of the scientific-research and technological plan of Roshydromet. The research was supported by the grant from the Saint-Petersburg State University No 93016972.

Appendix A. Supplementary materials

Appendix A.1. Weather types: the Vangengeim – Girs classification

Vangengeim – Girs classification is based on the analysis of hybrid-kinematic maps [Huth *et al.*, 2008].

The process of building a hybrid-kinematic map includes: registering the centers of cyclones and anticyclones, as well as positions of linear-like depressions and ridges from the daily synoptic pressure charts; drawing the demarcation line between the areas with high concentration of cyclones and depressions, and the areas with a high concentration of anticyclones and ridges. To reproduce kinematics of this process, trajectories of the baric formations are traced.

In 1933, G. Y. Vangengeim suggested a set of indices characterizing atmospheric circulation. He introduced the concept of an elementary synoptic process (ESP). ESP is an evolution of the atmospheric pressure field during which the geographic distribution of the sign of the pressure anomalies and the direction of the main air transports are preserved within the Atlantic-European sector. All ESP could be further clustered in three main types of atmospheric circulation patterns: the western (W), eastern (E) and meridional (C) circulation types. This description is based on Barashkova *et al.* [2015].

The particular feature of the western type (W) is characterized by low amplitudes of the tropospheric Rossby waves moving fast from west to east. The baric features also move eastwards: cyclones – in the polar and mid-latitudes, anticyclones – in the subtropics. The high-pressure belt in the subtropics and the low pressure belt further north are well pronounced. This configuration of the atmospheric pressure results in predominantly zonal atmospheric transport. As the meridional air-mass exchange weakens, negative temperature anomalies are observed in the polar regions (radiative cooling) and the positive ones – in tropical regions (radiative warming).

The meridional type (C) is characterized by a large amplitude of Rossby waves in the troposphere. The northwards transport of the warm air (to the Arctic) goes along the western sides of the pressure ridges, and the southwards transport (from the Arctic) is observed along the eastern sides. This leads to high zonal temperature contrasts, convergence of the high-altitude winds and dynamically linked growth of the sea-surface pressure. High temperature contrasts, characteristic for this weather type, forms favorable conditions for formation of sharp atmospheric fronts and an enhanced cyclonic activity. During the circulation type C, the Icelandic low is practically nonexistent due to a development of the high-pressure anomaly over the north Atlantic, the so called Atlantic Ridge. Further east, the Siberian Anticyclone strengthens and becomes connected with the Polar Anticyclone.

Similar to type C, the eastern type (E) is characterized by the large amplitude of tropospheric Rossby waves. However, the localization of ridges and troughs, as well as the distribution of the temperature anomalies, change to the opposite. Icelandic low is now well developed. The Scandinavian Ridge is formed, while the winter Siberian anticyclone weakens and shifts west.

Appendix A.2. Supplementary figures

As there is almost an infinite amount of variations of the transects positioning, it is impossible to give a full estimate of the connected uncertainties. We have performed a number of experiments, some of which are presented in the Figure A1. The results show that, though sometimes affecting the absolute values of the heat advection, the variations of the transect positions or of the reference temperature practically do not change neither the character of the interannual variability, nor the long-term trends, which are the focus of this study. Thus, when analyzing heat advection, one should be careful comparing absolute values of fluxes or budgets, but be rather confident in the derived tendencies and periodicities.

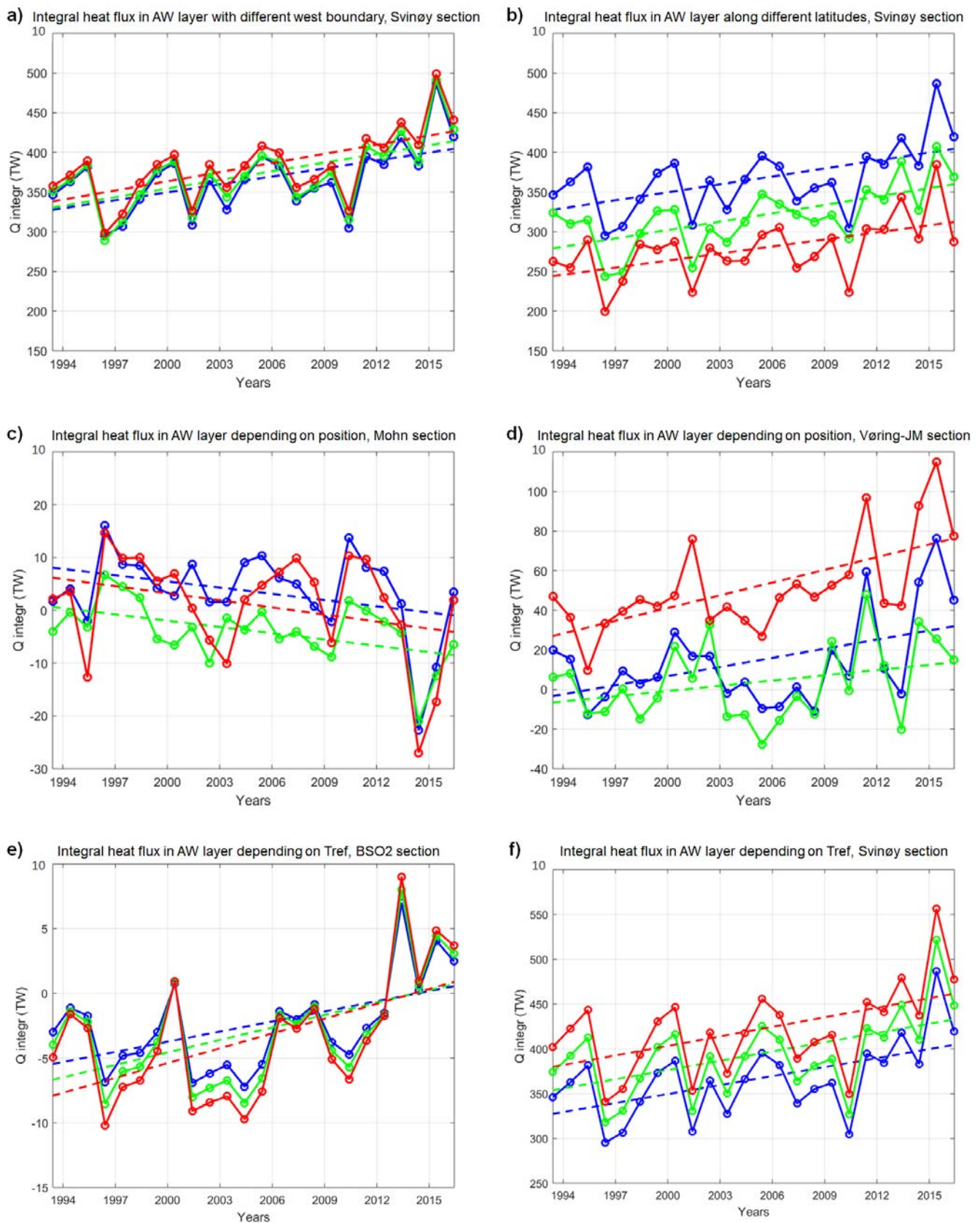


Figure A1. Examples of integral heat flux in the AW layer for different locations of the transects and different choices of the reference temperature.

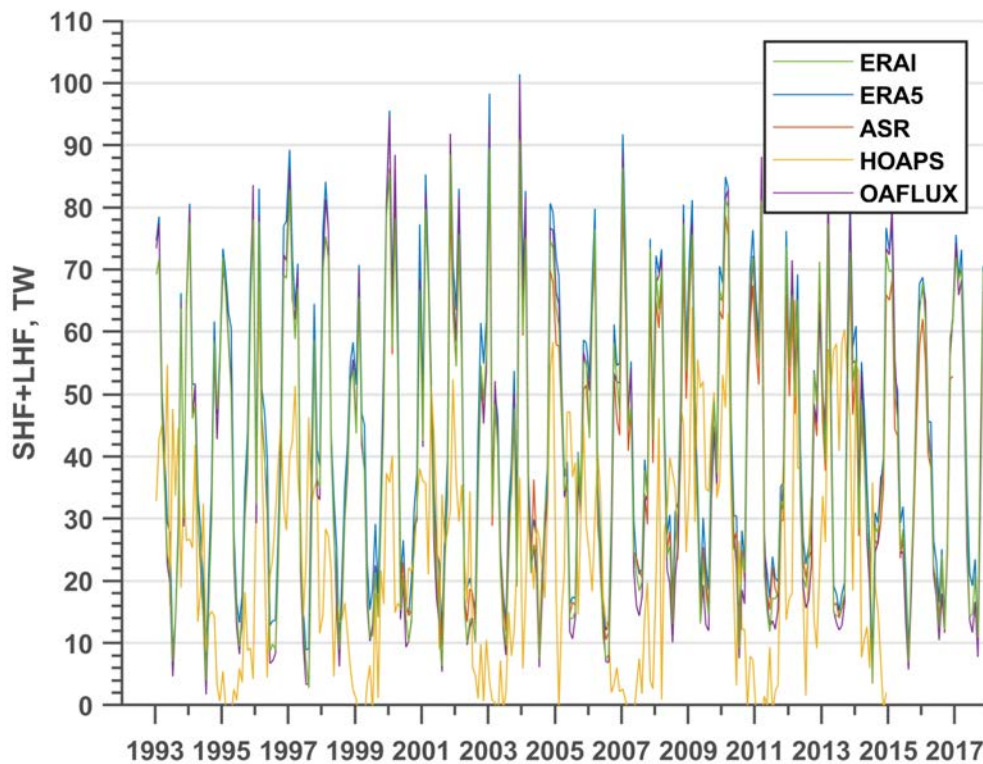


Figure A2. Ocean atmosphere heat exchange for region A, computed using different datasets.

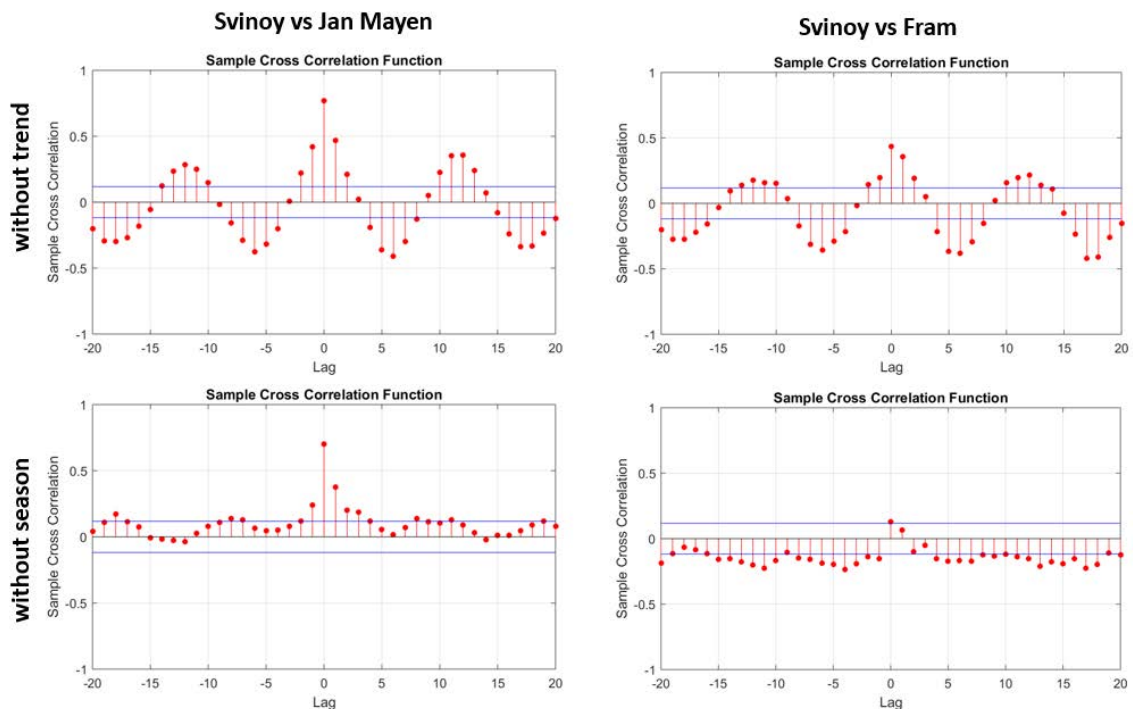


Figure A3. Example of the cross-correlations (lag in months) between the Svinøy – Jan Mayen sections (left) and Svinøy – Fram sections (right). The upper row s for the detrended time series, the lower row shows the correlations with the seasonal variability removed.

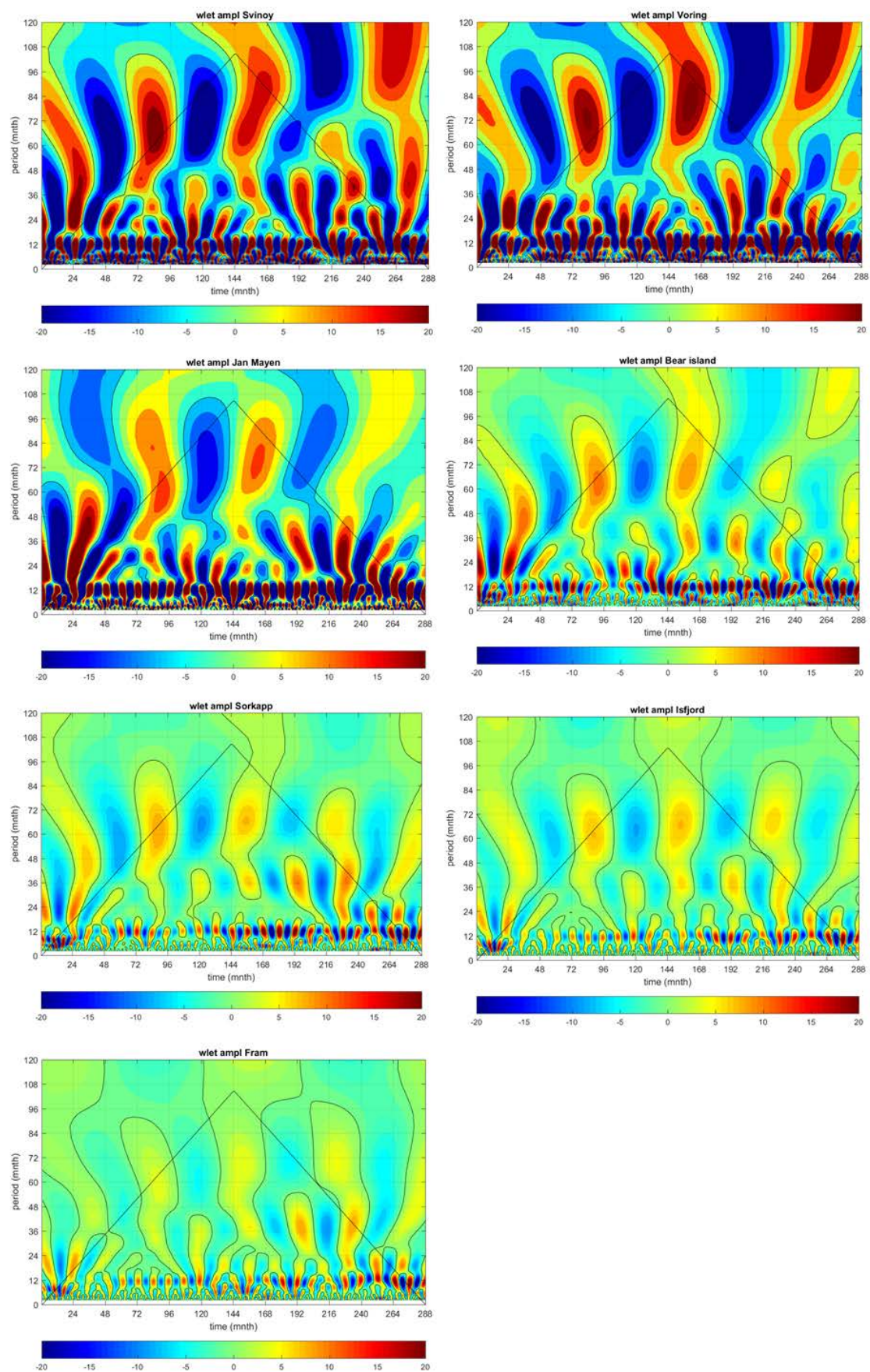


Figure A4. Wavelet diagrams of interannual variations of heat fluxes for the sections (right to left and up to down, see figure subtitles): Svinøy, Vøring, Jan Mayen, Bear Island, Sørkapp, Isfjord and Fram.

References

- Aagaard, K., A. Foldvik, and S. R. Hillman (1987), The West Spitsbergen Current: Disposition and water mass transformation, *Journal of Geophysical Research*, 92(C4), 3778–3784, <https://doi.org/10.1029/jc092ic04p03778>.
- Bacon, S., Y. Aksenov, S. Fawcett, and G. Madec (2015), Arctic mass, freshwater and heat fluxes: Methods and modelled seasonal variability, *Philosophical Transactions of the Royal Society A: Mathematical, Physical and Engineering Sciences*, 373(2052), 20140169, <https://doi.org/10.1098/rsta.2014.0169>.
- Barashkova, N. K., I. V. Kuzhevskaya, and D. V. Polyakov (2015), Classification of forms of atmospheric circulation: textbook (in Russian).
- Bashmachnikov, I. L., A. Y. Yurova, L. P. Bobylev, and A. V. Vesman (2018), Seasonal and Interannual Variations of Heat Fluxes in the Barents Sea Region, *Izvestiya, Atmospheric and Oceanic Physics*, 54(2), 213–222, <https://doi.org/10.1134/s001433818020032>.
- Bashmachnikov, I. L., I. E. Kozlov, L. A. Petrenko, N. I. Glok, and C. Wekerle (2020), Eddies in the North Greenland Sea and Fram Strait From Satellite Altimetry, SAR and High-Resolution Model Data, *Journal of Geophysical Research: Oceans*, 125(7), <https://doi.org/10.1029/2019jc015832>.
- Bashmachnikov, I. L., R. P. Raj, P. Golubkin, and I. E. Kozlov (2023), Heat Transport by Mesoscale Eddies in the Norwegian and Greenland Seas, *Journal of Geophysical Research: Oceans*, 128(2), 1–19, <https://doi.org/10.1029/2022jc018987>.
- Beszczynska-Möller, A., E. Fahrbach, U. Schauer, and E. Hansen (2012), Variability in Atlantic water temperature and transport at the entrance to the Arctic Ocean, 1997–2010, *ICES Journal of Marine Science*, 69(5), 852–863, <https://doi.org/10.1093/icesjms/fss056>.
- Beszczynska-Möller, A., W.-J. von Appen, and E. Fahrbach (2015), Physical oceanography and current meter data from moorings F1-F14 and F15/F16 in the Fram Strait, 1997–2012, <https://doi.org/10.1594/PANGAEA.150016>.
- Bezuglova, N. N., and G. S. Zinchenko (2009), Regional climatic manifestations of global atmospheric circulation in the south of Western Siberia, *Geography and Natural Resources*, 3, 83–87 (in Russian).
- Björk, G., B. G. Gustafsson, and A. Stigebrandt (2001), Upper layer circulation of the Nordic seas as inferred from the spatial distribution of heat and freshwater content and potential energy, *Polar Research*, 20(2), 161–168, <https://doi.org/10.3402/polar.v20i2.6513>.
- Bosse, A., I. Fer, H. Søiland, and T. Rossby (2018), Atlantic Water Transformation Along Its Poleward Pathway Across the Nordic Seas, *Journal of Geophysical Research: Oceans*, 123(9), 6428–6448, <https://doi.org/10.1029/2018jc014147>.
- Buckley, M. W., and J. Marshall (2016), Observations, inferences, and mechanisms of the Atlantic Meridional Overturning Circulation: A review, *Reviews of Geophysics*, 54(1), 5–63, <https://doi.org/10.1002/2015rg000493>.
- Carmack, E., I. Polyakov, L. Padman, I. Fer, E. Hunke, J. Hutchings, J. Jackson, D. Kelley, R. Kwok, C. Layton, H. Melling, D. Perovich, O. Persson, B. Ruddick, M.-L. Timmermans, J. Toole, T. Ross, S. Vavrus, and P. Winsor (2015), Toward Quantifying the Increasing Role of Oceanic Heat in Sea Ice Loss in the New Arctic, *Bulletin of the American Meteorological Society*, 96(12), 2079–2105, <https://doi.org/10.1175/bams-d-13-00177.1>.
- Chafik, L., J. Nilsson, Ø. Skagseth, and P. Lundberg (2015), On the flow of Atlantic water and temperature anomalies in the Nordic Seas toward the Arctic Ocean, *Journal of Geophysical Research: Oceans*, 120(12), 7897–7918, <https://doi.org/10.1002/2015jc011012>.
- Chafik, L., S. Häkkinen, M. H. England, J. A. Carton, S. Nigam, A. Ruiz-Barradas, A. Hannachi, and L. Miller (2016), Global linkages originating from decadal oceanic variability in the subpolar North Atlantic, *Geophysical Research Letters*, 43(20), 10,909–10,919, <https://doi.org/10.1002/2016gl071134>.
- Cokelet, E. D., N. Tervalon, and J. G. Bellingham (2008), Hydrography of the West Spitsbergen Current, Svalbard Branch: Autumn 2001, *Journal of Geophysical Research*, 113(C1), <https://doi.org/10.1029/2007jc004150>.

- Dee, D. P., S. M. Uppala, A. J. Simmons, P. Berrisford, P. Poli, S. Kobayashi, U. Andrae, M. A. Balmaseda, G. Balsamo, P. Bauer, P. Bechtold, A. C. M. Beljaars, L. van de Berg, J. Bidlot, N. Bormann, C. Delsol, R. Dragani, M. Fuentes, A. J. Geer, L. Haimberger, S. B. Healy, H. Hersbach, E. V. Hólm, L. Isaksen, P. Kållberg, M. Köhler, M. Matricardi, A. P. McNally, B. M. Monge-Sanz, J.-J. Morcrette, B.-K. Park, C. Peubey, P. de Rosnay, C. Tavolato, J.-N. Thépaut, and F. Vitart (2011), The ERA-Interim reanalysis: configuration and performance of the data assimilation system, *Quarterly Journal of the Royal Meteorological Society*, 137(656), 553–597, <https://doi.org/10.1002/qj.828>.
- Dickson, B., J. Meincke, and P. Rhines (2008), Arctic–Subarctic Ocean Fluxes: Defining the Role of the Northern Seas in Climate, in *Arctic-Subarctic Ocean Fluxes*, pp. 1–13, Springer Netherlands, https://doi.org/10.1007/978-1-4020-6774-7_1.
- Edson, J. B., V. Jampana, R. A. Weller, S. P. Bigorre, A. J. Plueddemann, C. W. Fairall, S. D. Miller, L. Mahrt, D. Vickers, and H. Hersbach (2013), On the Exchange of Momentum over the Open Ocean, *Journal of Physical Oceanography*, 43(8), 1589–1610, <https://doi.org/10.1175/jpo-d-12-0173.1>.
- Fahrbach, E. (2006), ASOF-N: Arctic-Subarctic Ocean Flux Array for European Climate: North, contract No: EVK2-CT-2002-00139; final report.
- Fairall, C. W., E. F. Bradley, J. E. Hare, A. A. Grachev, and J. B. Edson (2003), Bulk Parameterization of Air-Sea Fluxes: Updates and Verification for the COARE Algorithm, *Journal of Climate*, 16(4), 571–591, [https://doi.org/10.1175/1520-0442\(2003\)016<0571:bpoasf>2.0.co;2](https://doi.org/10.1175/1520-0442(2003)016<0571:bpoasf>2.0.co;2).
- Fedorov, A. M., I. L. Bashmachnikov, and T. V. Belonenko (2019), Winter convection in the Lofoten Basin according to ARGO buoys and hydrodynamic modeling, *Vestnik of Saint Petersburg University. Earth Sciences*, 64(3), 491–511, <https://doi.org/10.21638/spbu07.2019.308>.
- Fer, I., A. Bosse, B. Ferron, and P. Bouruet-Aubertot (2018), The Dissipation of Kinetic Energy in the Lofoten Basin Eddy, *Journal of Physical Oceanography*, 48(6), 1299–1316, <https://doi.org/10.1175/jpo-d-17-0244.1>.
- Furevik, T., C. Mauritzen, and R. Ingvaldsen (2007), The flow of Atlantic water to the Nordic Seas and Arctic Ocean, in *Arctic Alpine Ecosystems and People in a Changing Environment*, pp. 123–146, Springer, Berlin, Heidelberg, https://doi.org/10.1007/978-3-540-48514-8_8.
- Gascard, J.-C., and K. A. Mork (2008), Climatic Importance of Large-Scale and Mesoscale Circulation in the Lofoten Basin Deduced from Lagrangian Observations, in *Arctic-Subarctic Ocean Fluxes*, pp. 131–143, Springer, Dordrecht, https://doi.org/10.1007/978-1-4020-6774-7_7.
- Gascard, J.-C., C. Richez, and C. Rouault (1995), New insights on large-scale oceanography in Fram Strait: The West Spitsbergen Current, in *Coastal and Estuarine Studies*, pp. 131–182, American Geophysical Union, <https://doi.org/10.1029/ce049p0131>.
- Girs, A. A., and K. V. Kondratovich (1978), *Methods of long term weather forecasts*, 343 pp., Gidrometeoizdat, Leningrad (in Russian).
- Guinehut, S., P. Y. L. Traon, G. Larnicol, and S. Philipps (2004), Combining Argo and remote-sensing data to estimate the ocean three-dimensional temperature fields—a first approach based on simulated observations, *Journal of Marine Systems*, 46(1–4), 85–98, <https://doi.org/10.1016/j.jmarsys.2003.11.022>.
- Guinehut, S., A.-L. Dhomps, G. Larnicol, and P.-Y. L. Traon (2012), High resolution 3-D temperature and salinity fields derived from in situ and satellite observations, *Ocean Science*, 8(5), 845–857, <https://doi.org/10.5194/os-8-845-2012>.
- Hansen, B., S. Østerhus, W. R. Turrell, S. Jónsson, H. Valdimarsson, H. Hátún, and S. M. Olsen (2008), The Inflow of Atlantic Water, Heat, and Salt to the Nordic Seas Across the Greenland-Scotland Ridge, in *Arctic-Subarctic Ocean Fluxes*, pp. 15–43, Springer Netherlands, https://doi.org/10.1007/978-1-4020-6774-7_2.
- Huth, R., C. Beck, A. Philipp, M. Demuzere, Z. Ustrnul, M. Cahynová, J. Kyselý, and O. E. Tveito (2008), Classifications of Atmospheric Circulation Patterns: recent, advances and applications, *Annals of the New York Academy of Sciences*, 1146(1), 105–152, <https://doi.org/10.1196/annals.1446.019>.
- Jónsson, S., and H. Valdimarsson (2012), Water mass transport variability to the North Icelandic shelf, 1994–2010, *ICES Journal of Marine Science*, 69(5), 809–815, <https://doi.org/10.1093/icesjms/fss024>.

- Jungclauss, J. H., and T. Koenigk (2009), Low-frequency variability of the arctic climate: the role of oceanic and atmospheric heat transport variations, *Climate Dynamics*, 34(2-3), 265–279, <https://doi.org/10.1007/s00382-009-0569-9>.
- Kalavichchi, K. A., and I. L. Bashmachnikov (2019), Mechanism of a Positive Feedback in Long-Term Variations of the Convergence of Oceanic and Atmospheric Heat Fluxes and of the Ice Cover in the Barents Sea, *Izvestiya, Atmospheric and Oceanic Physics*, 55(6), 640–649, <https://doi.org/10.1134/s0001433819060173>.
- Kalavichchi, K. A., and I. L. Bashmachnikov (2021), Ocean-Atmosphere Interactions in the Barents Sea from Reanalyses Data, *Izvestiya, Atmospheric and Oceanic Physics*, 57(2), 159–169, <https://doi.org/10.1134/s0001433821020067>.
- Latarius, K., and D. Quadfasel (2016), Water mass transformation in the deep basins of the Nordic Seas: Analyses of heat and freshwater budgets, *Deep Sea Research Part I: Oceanographic Research Papers*, 114, 23–42, <https://doi.org/10.1016/j.dsr.2016.04.012>.
- Lenn, Y. D., P. J. Wiles, S. Torres-Valdes, E. P. Abrahamsen, T. P. Rippeth, J. H. Simpson, S. Bacon, S. W. Laxon, I. Polyakov, V. Ivanov, and S. Kirillov (2009), Vertical mixing at intermediate depths in the Arctic boundary current, *Geophysical Research Letters*, 36(5), <https://doi.org/10.1029/2008gl036792>.
- Lien, V. S., F. B. Vikebø, and Ø. Skagseth (2013), One mechanism contributing to co-variability of the Atlantic inflow branches to the Arctic, *Nature Communications*, 4(1), <https://doi.org/10.1038/ncomms2505>.
- Makhotin, M. S., and V. V. Ivanov (2016), Circulation of the Atlantic water in the Barents Sea based on hydrological survey data and numerical simulation, in *Hydrometeorological Research and Forecasting*, vol. 361, pp. 169–191, Hydrometcentre of Russia (in Russian).
- Moore, G. W. K., I. A. Renfrew, and R. S. Pickart (2012), Spatial distribution of air-sea heat fluxes over the sub-polar North Atlantic Ocean, *Geophysical Research Letters*, 39(18), <https://doi.org/10.1029/2012gl053097>.
- Mork, K. A., and J. Blindheim (2000), Variations in the Atlantic inflow to the Nordic Seas, 1955–1996, *Deep Sea Research Part I: Oceanographic Research Papers*, 47(6), 1035–1057, [https://doi.org/10.1016/s0967-0637\(99\)00091-6](https://doi.org/10.1016/s0967-0637(99)00091-6).
- Mork, K. A., and Ø. Skagseth (2010), A quantitative description of the Norwegian Atlantic Current by combining altimetry and hydrography, *Ocean Science*, 6(4), 901–911, <https://doi.org/10.5194/os-6-901-2010>.
- Mork, K. A., Ø. Skagseth, and H. Søiland (2019), Recent Warming and Freshening of the Norwegian Sea Observed by Argo Data, *Journal of Climate*, 32(12), 3695–3705, <https://doi.org/10.1175/jcli-d-18-0591.1>.
- Muilwijk, M., L. H. Smedsrud, M. Ilicak, and H. Drange (2018), Atlantic Water Heat Transport Variability in the 20th Century Arctic Ocean From a Global Ocean Model and Observations, *Journal of Geophysical Research: Oceans*, 123(11), 8159–8179, <https://doi.org/10.1029/2018jc014327>.
- Mulet, S., M.-H. Rio, A. Mignot, S. Guinehut, and R. Morrow (2012), A new estimate of the global 3D geostrophic ocean circulation based on satellite data and in-situ measurements, *Deep Sea Research Part II: Topical Studies in Oceanography*, 77–80, 70–81, <https://doi.org/10.1016/j.dsr2.2012.04.012>.
- Orvik, K. A., and P. Niiler (2002), Major pathways of Atlantic water in the northern North Atlantic and Nordic Seas toward Arctic, *Geophysical Research Letters*, 29(19), 1–4, <https://doi.org/10.1029/2002gl015002>.
- Orvik, K. A., Ø. Skagseth, and M. Mork (2001), Atlantic inflow to the Nordic Seas: current structure and volume fluxes from moored current meters, VM-ADCP and SeaSoar-CTD observations, 1995–1999, *Deep Sea Research Part I: Oceanographic Research Papers*, 48(4), 937–957, [https://doi.org/10.1016/s0967-0637\(00\)00038-8](https://doi.org/10.1016/s0967-0637(00)00038-8).
- Pacanowski, R. C., and S. G. H. Philander (1981), Parameterization of Vertical Mixing in Numerical Models of Tropical Oceans, *Journal of Physical Oceanography*, 11(11), 1443–1451, [https://doi.org/10.1175/1520-0485\(1981\)011<1443:povmin>2.0.co;2](https://doi.org/10.1175/1520-0485(1981)011<1443:povmin>2.0.co;2).
- Piechura, J., and W. Walczowski (2009), Warming of the West Spitsbergen Current and sea ice north of Svalbard, *OCEANOLOGIA*, 51(2), 147–164, <https://doi.org/10.5697/oc.51-2.147>.
- Polyakov, I. V., A. V. Pnyushkov, M. B. Alkire, I. M. Ashik, T. M. Baumann, E. C. Carmack, I. Goszczko, J. Guthrie, V. V. Ivanov, T. Kanzow, R. Krishfield, R. Kwok, A. Sundfjord, J. Morison, R. Rember, and A. Yulin (2017), Greater role for Atlantic inflows on sea-ice loss in the Eurasian Basin of the Arctic Ocean, <https://doi.org/10.1126/science.aai8204>.

- Poulain, P.-M., A. Warn-Varnas, and P. P. Niiler (1996), Near-surface circulation of the Nordic seas as measured by Lagrangian drifters, *Journal of Geophysical Research: Oceans*, 101(C8), 18,237–18,258, <https://doi.org/10.1029/96jc00506>.
- Prokhorova, U. V., P. N. Svyashchennikov, O. Nordli, K. Isaksen, H. M. Gjetlen, and E. J. Forland (), Investigation spatio temporal variability of atmospheric processes in Arctic regions, in *International Scientific and Practical Conference LXIX Herzen Readings April 21-23, 2016*, HERZEN UNIVERSITY (in Russian).
- Raj, R. P., J. E. Ø. Nilsen, J. A. Johannessen, T. Furevik, O. B. Andersen, and L. Bertino (2018), Quantifying Atlantic Water transport to the Nordic Seas by remote sensing, *Remote Sensing of Environment*, 216, 758–769, <https://doi.org/10.1016/j.rse.2018.04.055>.
- Raj, R. P., S. Chatterjee, L. Bertino, A. Turiel, and M. Portabella (2019), The Arctic Front and its variability in the Norwegian Sea, *Ocean Science*, 15(6), 1729–1744, <https://doi.org/10.5194/os-15-1729-2019>.
- Raj, R. P., I. Halo, S. Chatterjee, T. Belonenko, M. Bakhoday-Paskyabi, I. Bashmachnikov, A. Fedorov, and J. Xie (2020), Interaction Between Mesoscale Eddies and the Gyre Circulation in the Lofoten Basin, *Journal of Geophysical Research: Oceans*, 125(7), <https://doi.org/10.1029/2020jc016102>.
- Rosby, T., C. Flagg, L. Chafik, B. Harden, and H. Søiland (2018), A Direct Estimate of Volume, Heat, and Freshwater Exchange Across the Greenland-Iceland-Faroe-Scotland Ridge, *Journal of Geophysical Research: Oceans*, 123(10), 7139–7153, <https://doi.org/10.1029/2018jc014250>.
- Rudels, B. (1987), *On the mass balance of the Polar Ocean, with special emphasis on the Fram Strait*, Norsk polarinstitutt, Oslo.
- Rudels, B. (2015), Arctic Ocean circulation, processes and water masses: A description of observations and ideas with focus on the period prior to the International Polar Year 2007-2009, *Progress in Oceanography*, 132, 22–67, <https://doi.org/10.1016/j.pocean.2013.11.006>.
- Rudels, B., U. Schauer, G. Björk, M. Korhonen, S. Pisarev, B. Rabe, and A. Wisotzki (2013), Observations of water masses and circulation with focus on the Eurasian Basin of the Arctic Ocean from the 1990s to the late 2000s, *Ocean Science*, 9(1), 147–169, <https://doi.org/10.5194/os-9-147-2013>.
- Saloranta, T. M., and P. M. Haugan (2004), Northward cooling and freshening of the warm core of the West Spitsbergen Current, *Polar Research*, 23(1), 79–88, <https://doi.org/10.1111/j.1751-8369.2004.tb00131.x>.
- Schauer, U., and A. Beszczynska-Möller (2009), Problems with estimation and interpretation of oceanic heat transport - conceptual remarks for the case of Fram Strait in the Arctic Ocean, *Ocean Science*, 5(4), 487–494, <https://doi.org/10.5194/os-5-487-2009>.
- Schauer, U., E. Fahrbach, S. Osterhus, and G. Rohardt (2004), Arctic warming through the Fram Strait: Oceanic heat transport from 3 years of measurements, *Journal of Geophysical Research*, 109(C6), <https://doi.org/10.1029/2003jc001823>.
- Schauer, U., A. Beszczynska-Möller, W. Walczowski, E. Fahrbach, J. Piechura, and E. Hansen (2008), Variation of Measured Heat Flow Through the Fram Strait Between 1997 and 2006, in *Arctic-Subarctic Ocean Fluxes*, pp. 65–85, Springer Netherlands, https://doi.org/10.1007/978-1-4020-6774-7_4.
- Schlichtholz, P. (2011), Influence of oceanic heat variability on sea ice anomalies in the Nordic Seas, *Geophysical Research Letters*, 38(5), <https://doi.org/10.1029/2010gl045894>.
- Schlichtholz, P. (2013), Observational Evidence for Oceanic Forcing of Atmospheric Variability in the Nordic Seas Area, *Journal of Climate*, 26(9), 2957–2975, <https://doi.org/10.1175/jcli-d-11-00594.1>.
- Segtnan, O. H., T. Furevik, and A. D. Jenkins (2011), Heat and freshwater budgets of the Nordic seas computed from atmospheric reanalysis and ocean observations, *Journal of Geophysical Research: Oceans*, 116(C11), <https://doi.org/10.1029/2011jc006939>.
- Sirevaag, A., and I. Fer (2012), Vertical heat transfer in the Arctic Ocean: The role of double-diffusive mixing, *Journal of Geophysical Research: Oceans*, 117(C7), <https://doi.org/10.1029/2012jc007910>.
- Skagseth, Ø., K. A. Orvik, and T. Furevik (2004), Coherent variability of the Norwegian Atlantic Slope Current derived from TOPEX/ERS altimeter data, *Geophysical Research Letters*, 31(14), <https://doi.org/10.1029/2004gl020057>.

- Skagseth, Ø., T. Furevik, R. Ingvaldsen, H. Loeng, K. A. Mork, K. A. Orvik, and V. Ozhigin (2008), Volume and Heat Transports to the Arctic Ocean Via the Norwegian and Barents Seas, in *Arctic-Subarctic Ocean Fluxes*, pp. 45–64, Springer Netherlands, https://doi.org/10.1007/978-1-4020-6774-7_3.
- Skagseth, Ø., K. F. Drinkwater, and E. Terrile (2011), Wind- and buoyancy-induced transport of the Norwegian Coastal Current in the Barents Sea, *Journal of Geophysical Research*, 116(C8), <https://doi.org/10.1029/2011jc006996>.
- Smedsrud, L. H., R. Ingvaldsen, J. E. Ø. Nilsen, and Ø. Skagseth (2010), Heat in the Barents Sea: transport, storage, and surface fluxes, *Ocean Science*, 6(1), 219–234, <https://doi.org/10.5194/os-6-219-2010>.
- Smedsrud, L. H., I. Esau, R. B. Ingvaldsen, T. Eldevik, P. M. Haugan, C. Li, V. S. Lien, A. Olsen, A. M. Omar, O. H. Otterå, B. Risebrobakken, A. B. Sandø, V. A. Semenov, and S. A. Sorokina (2013), The role of the Barents Sea in the Arctic climate system, *Reviews of Geophysics*, 51(3), 415–449, <https://doi.org/10.1002/rog.20017>.
- Taylor, K. E. (2001), Summarizing multiple aspects of model performance in a single diagram, *Journal of Geophysical Research: Atmospheres*, 106(D7), 7183–7192, <https://doi.org/10.1029/2000jd900719>.
- Timmermann, R., and A. Beckmann (2004), Parameterization of vertical mixing in the Weddell Sea, *Ocean Modelling*, 6(1), 83–100, [https://doi.org/10.1016/s1463-5003\(02\)00061-6](https://doi.org/10.1016/s1463-5003(02)00061-6).
- Torrence, C., and G. P. Compo (1998), A Practical Guide to Wavelet Analysis, *Bulletin of the American Meteorological Society*, 79(1), 61–78, [https://doi.org/10.1175/1520-0477\(1998\)079<0061:apgtwa>2.0.co;2](https://doi.org/10.1175/1520-0477(1998)079<0061:apgtwa>2.0.co;2).
- Tverberg, V., O. A. Nøst, C. Lydersen, and K. M. Kovacs (2014), Winter sea ice melting in the Atlantic Water subduction area, Svalbard Norway, *Journal of Geophysical Research: Oceans*, 119(9), 5945–5967, <https://doi.org/10.1002/2014jc010013>.
- Vangengeim, G. Y. (1933), Application of Synoptic Methods to the Study and Characterization of Climate, *Izvestia GGO*, 2, 3–16 (in Russian).
- Verbrugge, N., S. Mulet, S. Guinehut, and B. Buongiorno-Nardelli (2017), ARMOR3D: A 3D multi-observations T,S,U,V product of the ocean, in *19th EGU General Assembly, EGU2017, proceedings from the conference held 23–28 April, 2017*, vol. 19, p. 17579, EGU.
- Vesman, A. V., B. V. Ivanov, and V. A. Volkov (2017), Changes in thermohaline system on the west Spitsbergen shelf since 1950 to present time, *Czech Polar Reports*, 7(1), 62–73, <https://doi.org/10.5817/cpr2017-1-7>.
- von Appen, W.-J., U. Schauer, R. Somavilla, E. Bauerfeind, and A. Beszczynska-Möller (2015), Exchange of warming deep waters across Fram Strait, *Deep Sea Research Part I: Oceanographic Research Papers*, 103, 86–100, <https://doi.org/10.1016/j.dsr.2015.06.003>.
- Walczowski, W. (2014), *Atlantic Water in the Nordic Seas*, vol. 13, <https://doi.org/10.1007/978-3-319-01279-7>.
- Wekerle, C., Q. Wang, W.-J. von Appen, S. Danilov, V. Schourup-Kristensen, and T. Jung (2017), Eddy-Resolving Simulation of the Atlantic Water Circulation in the Fram Strait With Focus on the Seasonal Cycle, *Journal of Geophysical Research: Oceans*, 122(11), 8385–8405, <https://doi.org/10.1002/2017jc012974>.